Environmental Science & Technology

pubs.acs.org/est

Article

Disentangling Near-Road Emission Inequities in Hong Kong through Data-Driven Spatiotemporal Traffic Dynamics

Chenming Niu, Qiuzi Chen, An Wang, and Junshi Xu*

Cite This: https://doi.org/10.1021/acs.est.5c14619

Read Online

ACCESS | Metrics & More | Article Recommendations | Supporting Information

ABSTRACT: Traffic emissions contribute disproportionately to exposure inequities in dense cities. Delivery fleets and public buses can intensify these burdens in vulnerable communities, yet most assessments overlook such dynamics by aggregating fleets into broad categories and averaging across the day. This obscures when and which vehicles drive inequities. We developed a vehicle-class and hour-resolved approach for Hong Kong to estimate traffic emissions. We integrated high-resolution traffic counts, street imagery, and detector data with machine learning and computer vision to model hourly NO_x and $PM_{2.5}$ for all road segments during typical daily activity hours. The framework explains over 95% of the variance in NO_x and $PM_{2.5}$ emissions. Results show substantial traffic-related emission inequities in Hong Kong, with low-income residents experiencing 8%−9% higher NO_x levels than high-income residents, and Chinese residents experiencing 40%−52% higher NO_x levels than White residents. The dominant contributors shift over the day, with delivery fleets driving daytime inequities and franchised buses amplifying evening inequities. Across all hours, light-duty goods vehicles contribute 31−35% of disparities, franchised buses 25−35%, and heavy-duty goods vehicles 19−23%, varying by population group. This study provides one of the first data-driven analyses of vehicle-specific impacts, revealing when and which vehicles drive inequities and guiding equity-focused interventions.

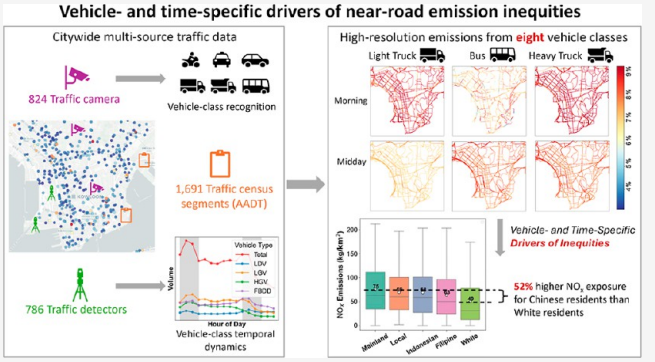

KEYWORDS: *vehicle-class dynamics, fine-scale traffic emissions, source-resolved disparities, spatiotemporal modeling, environmental justice, machine learning*

1. INTRODUCTION

Exposure disparities related to traffic pollution remain a persistent environmental justice concern in high-density cities,[1−9] where residential neighborhoods are situated near major transport corridors.[1] Freight and passenger fleets operate intensively within these mixed-use environments, contributing to elevated and time-varying pollution levels that affect nearby residents throughout the day.[8,10] These nearby residents are disproportionately composed of socioeconomically disadvantaged or marginalized groups, who face heightened health risks due to their cumulative exposure to traffic-related air pollutants formed from primary vehicle emissions.[2,6,7,11−14] This underscores the need for targeted interventions to reduce the unequal exposure burden of marginalized populations.

Designing targeted interventions requires identifying where and when traffic-related pollution burdens are highest and which vehicle classes contribute most. High spatial and temporal resolution is critical for this need, because traffic emissions can vary sharply over short road segments and across hours due to the heterogeneity in traffic composition and activity.[13,15−18] Spatial aggregation can obscure near-road pollution hotspots that are most relevant to population exposure, while temporal averaging can mask peak-emission periods that coincide with high travel activity.[19] Coarse-resolution approaches may therefore underestimate the magnitude of traffic-related exposure disparities and cannot identify the vehicle sources most relevant for mitigation.

Research on traffic-related exposure disparities has progressed through both measurement-based[8,9,20−22] and modeling approaches.[5,6,23−27] Measurement studies, including fixed-site[8] and mobile monitoring,[9,22] provide direct evidence of pollutant concentrations but differ substantially in their spatial and temporal coverage. Fixed-site monitoring offers long-term, high-frequency records yet lacks spatial detail and near-road representativeness.[8,28] Mobile monitoring, in contrast, provides extensive spatial coverage and enables estimation of annual-average exposure levels based on measured pollutant

Received: October 15, 2025
Revised: March 1, 2026
Accepted: March 3, 2026

concentrations, but cannot resolve diurnal variability due to its limited sampling duration.[29−31] While these measurement approaches form the empirical foundation for understanding near-road air quality, their limitations highlight the need for frameworks that can extend observations across broader spatial and temporal scales.

Beyond direct measurements, modeling approaches are widely applied to estimate population exposure to traffic-related air pollution.[5,6,16,27] Modeling approaches often integrate traffic simulation outputs to represent vehicle activity with proximity-based metrics[6,32] or chemical transport models[5,33−36] to assess exposure across urban networks. They capture broader spatial and temporal patterns than measurements, providing valuable insights into population-level disparities. However, their accuracy depends on the quality of input data and assumptions regarding traffic activity,[6] fleet composition,[6,8,37] and emission factors, which are often generalized or outdated. Conventional frameworks struggle to capture fine-scale heterogeneity and short-term variation, both critical for understanding localized exposure inequities. These limitations prompted a shift toward data-driven approaches leveraging multisource traffic and environmental data to improve accuracy and interpretability.[8,23,29−31]

Both measurement and modeling studies in environmental justice consistently show that disadvantaged groups, including low-income and minority populations, experience higher exposure to traffic-related air pollution than wealthier groups.[5−8,11,38−41] However, most work has focused on quantifying exposure disparities rather than identifying how specific traffic emission sources contribute to these disparities. This gap stems from reliance on temporally aggregated data and broad vehicle classifications, which obscure how specific fleet types contribute to inequities across space and time.

In Hong Kong, this limitation can mask substantial heterogeneity because road activity is not solely driven by private cars, and diesel-powered buses and trucks operate intensively in mixed-use corridors.[42,43] Although heavy-duty trucks were often identified as dominant contributors due to their higher per-vehicle emission rates and intensive operation along major corridors in environmental justice research,[5,6,44,45] light-duty trucks and buses have received less attention. Heavy-duty trucks generally refer to freight vehicles with high gross vehicle weights (≥11.8 tonnes in the United States and ≥15 tonnes in Hong Kong), such as long-haul trucks and container vehicles, whereas light-duty trucks include small delivery vehicles, such as vans and pickup trucks. In transit-dependent port cities such as Hong Kong, light-duty trucks and public buses can play a larger role in freight activity and passenger travel than in more car-oriented contexts such as the United States. The distinct spatial and temporal operating patterns of these vehicles can align with peak population presence in residential or transit-dense areas, intensifying inequities and highlighting the need for vehicle- and time-resolved analysis.

Capturing these spatiotemporal dynamics requires methods capable of resolving emissions and exposures with fine spatial, temporal, and fleet-specific detail. Recent advances in data science have introduced promising alternatives to conventional modeling frameworks by enabling richer integration of diverse data sources. Machine-learning algorithms can estimate traffic volumes, emissions, and pollutant concentrations efficiently across large and complex urban networks.[6,8,31,46−50] Computer-vision techniques can extract detailed vehicle characteristics and activity patterns from street-level imagery.[30,51] Reported classification performance varies across vehicle classes and imaging conditions. For example, a street-view computer-vision model developed for mobile monitoring detected and classified ten vehicle categories with an average precision of approximately 59%, with higher accuracy for common vehicle types.[30] When combined, these data science approaches provide a comprehensive and scalable framework for characterizing how exposure disparities emerge and evolve across space, time, and heterogeneous vehicle fleets in urban environments.

Building on the technique advances, this study offers a new perspective on environmental justice by examining how urban traffic dynamics shape emission-related exposure disparities in Hong Kong, a dense Asian city with complex transport systems and notable social inequalities. Moving beyond aggregate assessments, we resolve variations in traffic emissions across vehicle classes and times of day to identify when and which fleets most intensify inequities in an emission-based exposure indicator. The framework advances understanding of how spatial and temporal traffic patterns drive unequal exposure risks and provides an empirical basis for designing targeted, equity-oriented mitigation strategies in complex urban environments.

2. METHODS

2.1. Study Area and Traffic Data

Hong Kong provides an ideal setting for investigating transport-related environmental justice because of its compact urban form, high population density, and wide income disparities, which can produce strong spatial contrasts in exposures. The city's 7.4 million residents live within 1104 km^2, yet only about 20% of the land is zoned for residential and commercial use.[52] Nearly half of residents live in public housing for low-income households, many of which are located within 100 m of major transport corridors.[53] Income inequality has continued to widen, with the ratio between the richest and poorest deciles increasing from 34.3 in 2019 to 81.9 in 2024,[54] intensifying socioeconomic inequality.

The city's transport system reflects its compact urban form and limited land availability. As a major port city, Hong Kong relies heavily on logistics activity for freight movement and on public transit for daily commuting. Although private cars constituted about 71% of Hong Kong's licensed vehicles in 2021,[55] they account for only about 12% of total daily trips and approximately 54% of total traffic volumes according to Cross-harbor Traffic Statistic.[56] In contrast, franchised buses made up less than 1% of licensed vehicles yet carried nearly 27% of all daily trips.[42] Given that emission factors for buses and goods vehicles are substantially higher than those for private cars, this discrepancy between fleet composition and traffic activity can generate pronounced heterogeneity in vehicle-class contributions to traffic emissions. In Hong Kong's 2023 emission inventory,[57] road transport accounts for about 17% of total NO_x and 12% of total $PM_{2.5}$ emissions. Although this represents a relatively modest contribution in aggregate, vehicle emissions are released at street level in proximity to residents and pedestrians, and can therefore dominate near-road concentration gradients and contribute to spatial disparities in population exposure.

To capture the dynamics of traffic emissions, three data sets were integrated to characterize traffic activity across the urban road network: (1) annual average daily traffic (AADT) data for 2023 obtained from the Transport Department's traffic census,[56] covering 1691 road segments classified by road type and georeferenced using coordinates, names, and directions; (2) vehicle class information derived from still images captured by 987 public traffic cameras between July and August 2024,[58] where after excluding poor-quality sites (Figure S1), 824 valid locations remained, yielding over 17 million usable images; and (3) speed and volume data from 786 loop

https://doi.org/10.1021/acs.est.5c14619
Environ. Sci. Technol. XXXX, XXX, XXX−XXX

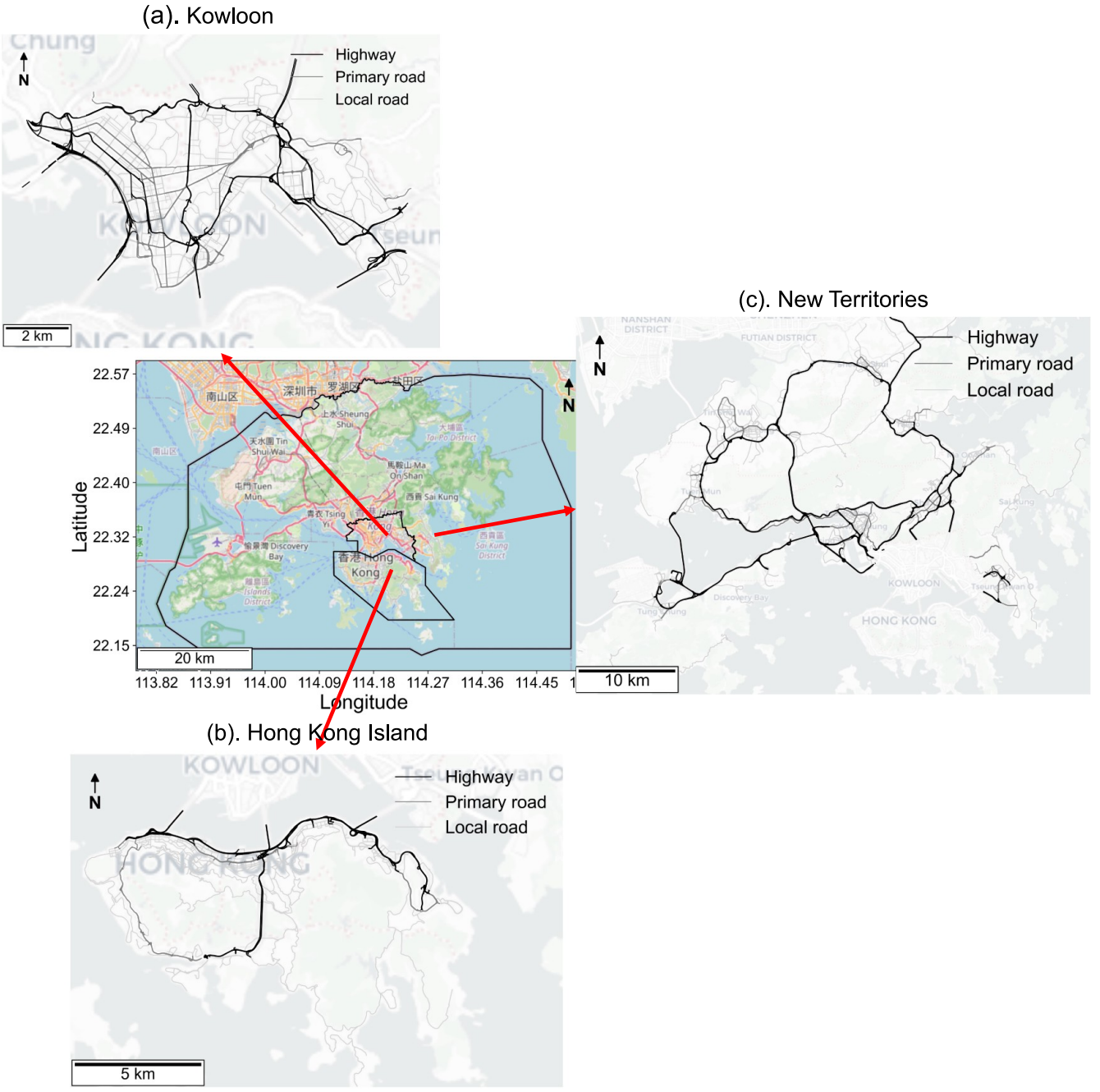

Figure 1. Spatial context of the study area and regional road networks in Hong Kong. The central panel shows the boundaries of the three administrative regions, Kowloon, Hong Kong Island, and the New Territories. Surrounding panels present the road networks within each region: (a) Kowloon, (b) Hong Kong Island, and (c) the New Territories. Roads are classified by functional hierarchy (highways, primary, and local roads).

detectors operating at 60 s intervals throughout 2023,[59] aggregated to hourly averages to represent annual traffic conditions.

Among the AADT samples, 169 (10.0%) are located on highways, 322 (19.1%) on primary roads, and 1200 (70.9%) on local roads. Highways include both highways and trunk roads that serve interregional travel across Hong Kong, while local roads primarily consist of secondary and tertiary roads that connect residential neighborhoods within regions. The spatial context of Hong Kong and regional road networks is shown in Figure 1. The spatial distributions of population density and road network in Hong Kong are provided in Figure S2 for contextual reference. The spatial distributions of all three data sets are shown in Figure S3. Together, they form the basis for vehicle detection, classification, and traffic distribution modeling, enabling near-real-time emission estimation and data-driven traffic interventions.

2.2. Vehicle Detection and Classification via Computer Vision

Vehicles were classified into eight categories following definitions from the Hong Kong Transport Department[60] and the EMFAC-HK model:[61] motorcycle, private car, taxi, light-duty bus (LDB), heavy-duty bus (HDB), franchised double-deck bus (FBDD), light-duty goods vehicle (LGV), and heavy-duty goods vehicle (HGV). Detailed class descriptions and representative examples are provided in Table S1. In Hong Kong, LGVs typically refer to van-type vehicles used for parcel or food delivery, whereas HGVs refer to medium- to heavy-

https://doi.org/10.1021/acs.est.5c14619
Environ. Sci. Technol. XXXX, XXX, XXX−XXX

duty trucks for transporting bulk freight such as construction materials.

Images from traffic cameras were manually annotated by human annotators to identify vehicle bounding boxes and corresponding categories. For each camera, image sampling was conducted at 2 h intervals, yielding 12 images per site and a total of 7959 images after removing invalid ones. All 7959 retained images were fully labeled and subsequently divided into training, validation, and testing sets in a 5:2.5:2.5 ratio. To simulate different weather conditions, four augmentation types (fog, rain, shadow, and sun glare) were applied to the training set (Figure S4). A transfer learning approach was then used to fine-tune a YOLOv10x model for vehicle classification.[62] YOLOv10x is a one-stage convolutional neural network optimized for large-scale, real-time object detection, with demonstrated advantages in processing efficiency and accuracy for dense urban scenes. The high efficiency of YOLOv10x makes it well-suited for surveillance-based traffic monitoring applications that require processing large volumes of images, over 17 million in our case.

Two hyperparameters, epochs and batch size, were optimized while others remained at default values. The best configuration consisted of 300 epochs (with early stopping at 145) and a batch size of 16, evaluated using mean average precision. Model performance was validated on a 25% holdout test set, achieving an average precision of 78.3%, a recall of 78.9%, and a mean average precision at IoU = 0.5 (mAP50) of 82.7% across all classes. Further details on augmentation, fine-tuning, and per-class performance are provided in Supporting Information and Table S2.

The trained YOLOv10x was then applied to more than 17 million unlabeled traffic-camera images to detect and classify vehicles. Detection results were aggregated at the hourly level to estimate vehicle class proportions. For example, private cars represented about 70% of all detected vehicles between 7:00 and 8:00 a.m. Overall, the computer vision model is used to reconstruct observed hourly fleet composition patterns at the monitored camera locations during the study period. These hourly class proportions for each monitored link serve as empirical inputs for estimating road-segment-level vehicle class proportions across the network, as described in Section 2.3.

To further evaluate the reliability of the image-based vehicle classification, the derived hourly vehicle class proportions were compared with independent traffic survey data collected at 19 locations across Hong Kong.[56] At these sites, trained surveyors conducted one-day manual counts of vehicle volumes by class. Our estimated vehicle proportions showed good agreement with the survey-based observations, with average residuals (estimated proportion minus manually counted proportion) across the eight vehicle classes ranging from −7.51% to 7.62%.

2.3. Modeling Traffic Characteristics with Spatial Predictors

A series of XGBoost models, which are gradient boosting decision tree-based machine learning algorithms well suited for capturing nonlinear relationships and complex feature interactions,[63] were developed to estimate AADTs, hourly vehicle class proportions, hourly volume proportions, and hourly average speeds for each road segment between 7:00 a.m. and 11:00 p.m., using the spatial predictors described in Section 2.3.1. This time window was selected based on the travel characteristics survey (TCS),[42] which indicates that more than 95% of daily trips occur within this time frame. The hourly volume of each vehicle class on a road segment was calculated as the product of the modeled AADT, hourly volume proportion, and corresponding class proportion.

2.3.1. Spatial Predictors. To estimate AADT, we extracted a suite of independent variables describing road characteristics, network connectivity, land use, demographics, roadside infrastructure, and point-of-interest (POI) densities. Previous studies have shown that these factors correlate strongly with total traffic volume and AADT.[6,46,64] To improve model performance under Hong Kong's dense and vertically layered transport system, three additional context-specific predictors were developed.

First, the volumes of FBDDs and green minibuses (GMBs, a major subtype of LDBs) were estimated by reconstructing bus routes and frequencies using general transit feed specification (GTFS) data[65,66] (Figure S5). The GTFS bus dispatch table provides daily dispatch schedules for every bus route, including stop locations and scheduled arrival times. Bus stops were matched to network nodes, and paths between consecutive stops were identified using Dijkstra's algorithm.[67] This process was repeated for all bus dispatches, and the resulting paths were used to compute hourly bus volumes on each road segment, later serving as reference data for model refinement.

Second, as in many other high-density cities, Hong Kong's combination of compact urban form and extensive elevated highways means that local roads located beneath or adjacent to these corridors often carry lower traffic volumes than other roads of the same classification. To account for this, we calculated the proportion of each road segment overlapping with highways using buffer radii ranging from 10 to 50 m. Third, detector-related features, including detector density, daily detected vehicle counts, and daily average speed, were extracted within buffers of 500 m to 5000 m at 500 m intervals.

To estimate hourly volume proportions, vehicle class proportions, and speeds, the above spatial features were combined with hourly traffic data from the three nearest detectors, resulting in 48 additional variables. These features were used to capture local diurnal variation through interaction effects in the gradient boosting models. A full summary of all predictors and their data sources is provided in Table S3.

2.3.2. Model Evaluation and Refinement. Building upon the modeling framework described in Section 2.3.1, four types of traffic-related data were modeled to quantify hourly traffic volumes and emissions for each vehicle class across all road segments: AADT, hourly volume proportions, hourly vehicle class proportions, and hourly average speeds. Each data set was randomly divided, with 80% used for model training and 20% reserved for testing to evaluate individual model performance. Prior to model training, AADT values were log-transformed to reduce right skewness and limit the influence of extreme AADT values on model performance. Although this transformation improves overall model stability, XGBoost may still attenuate extreme observations due to its inherent robustness to outliers. This trade-off is considered acceptable as the primary objective of the model is to capture the network-wide traffic distributions.

To verify model accuracy and assess error propagation across modeling stages, we conducted an end-to-end validation using a randomly selected 10% subset of road segments with held-out observations ("ground truth"). Here, ground truth refers to observed AADTs, hourly volume proportions, vehicle class proportions, and speeds, which together allow the calculation of reference emissions. These reference emissions were then compared with emissions computed using model-estimated inputs. The spatial distribution of the validated segments is shown in Figure S6 and demonstrates broad coverage across Hong Kong, including Hong Kong Island (20.73%), Kowloon (42.12%), and New Territories (34.15%).

Evaluation metrics included the coefficient of determination (R^2), root mean squared error (RMSE), mean absolute error (MAE), and mean absolute percentage error (MAPE). Hyperparameters were tuned via grid search on the training set, with optimal values selected based on the lowest average RMSE from 5-fold cross-validation (details provided in the Supporting Information, Tables S4 and S5). To mitigate the potential overfitting arising from a large and correlated feature set, the L1 and L2 regularization hyperparameters were specifically tuned to constrain model complexity and limit the influence of redundant predictors. The final models with the best hyperparameters were applied to estimate traffic volumes and corresponding NO_x and $PM_{2.5}$ emissions across all road segments in Hong Kong.

To improve the accuracy of FBDD estimates, GTFS data were used to reconstruct bus routes, frequencies, and dispatch schedules. As franchised bus operations follow fixed timetables with regulated adherence, GTFS data offer a more reliable and temporally consistent

https://doi.org/10.1021/acs.est.5c14619
Environ. Sci. Technol. XXXX, XXX, XXX−XXX

record of service activity than image-based detections or model predictions. The GTFS-derived hourly volumes were therefore treated as representative of actual conditions. According to the Hong Kong Transport Department, the lost trip rate, defined as scheduled stops not operated, was only 2.7% in the first half of 2023,[68] indicating minimal deviation from scheduled service. The estimated volumes of the remaining seven vehicle classes were then proportionally scaled to preserve total hourly traffic volumes across all road segments, such that the sum of class-specific volumes matched the total estimated hourly volumes after replacing FBDD volumes with GTFS-derived volumes. The quantitative scaling procedure is detailed in the Supporting Information.

To assess the sensitivity of traffic volume estimates to the proportional adjustment applied to the remaining vehicle classes, two tests were conducted. First, we compared the traffic volumes without rescaling with those after adjustment. Second, to account for potential deviations from scheduled bus services, we simulated a network-wide lost-trip scenario by reducing GTFS-derived FBDD volumes to 97.3% of their baseline values and proportionally adjusted the volumes of other vehicle classes. Results of these assessments are summarized in Section 3.1.

2.4. Emission Calculation

Hourly NO_x and $PM_{2.5}$ emissions for each of the eight vehicle classes on every road segment in 2023 were estimated using the EMFAC-HK model.[61] EMFAC-HK is a Hong Kong-specific emission factor model adapted from the EMFAC framework originally developed by the California Air Resources Board (CARB), with further localization for Hong Kong vehicle fleet composition, activity patterns, and ambient conditions by the Hong Kong Environmental Protection Department. The model has been evaluated against real-world tunnel measurements in Hong Kong and shows good agreement for the 2015 fleet, with fleet-average emission factors differing by approximately 3% for $PM_{2.5}$ and 16% for NO_x.[69] Although EMFAC-HK is a cycle-based model and average speed inputs cannot fully capture second-by-second driving dynamics (e.g., acceleration and deceleration), its explicit representation of local fleet characteristics and strong empirical evaluation support its application for network-wide emission estimation.

Required inputs for EMFAC-HK include meteorological conditions, hourly traffic speeds, local fleet composition, and vehicle model year. Average hourly temperature and relative humidity for 2023 were obtained from the Hong Kong Observatory.[70] Hourly traffic speeds estimated by the XGBoost models were applied as inputs to EMFAC-HK.

EMFAC-HK incorporates the fuel-type composition within each vehicle class when generating emission factors, based on vehicle registration data from the Hong Kong Transport Department. In Hong Kong, private cars are predominantly gasoline-fueled, most franchised buses and goods vehicles use diesel, taxis and public light buses primarily use liquefied petroleum gas, and electric vehicles represent a growing share, mainly among private cars and taxis.[71]

EMFAC-HK divides LDB, HDB, LGV, and HGV into three to four subcategories based on gross vehicle weight (e.g., LGV_1 < 2.5 tonnes, LGV_2 = 2.5−3.5 tonnes), respectively.[61] Because the fine-tuned YOLOv10x model identified vehicles by class rather than by weight, the emission factors of subcategories were aggregated into a single representative value for each class using fleet composition data from the TCS.[43]

Using the above-mentioned inputs, EMFAC-HK generated hourly emission factors for NO_x and $PM_{2.5}$ (in g/km) by vehicle type and speed. The emission factors applied in this study represent running tailpipe exhaust emissions during on-road travel. Total emissions for each road segment l at each hour h were calculated using eq 1

$$E_{lht} = \sum_{k \in K} V_{lhk} \times \mathrm{RL}_l \times \mathrm{EF}_{hkt}, \qquad \forall\, l \in L,\, h \in H \tag{1}$$

where E_{lht} represents the emission of pollutant type $t \in \{NO_x, PM_{2.5}\}$ on road segment l at hour h; V_{lhk} is the estimated traffic volume of vehicle class k on segment l at hour h; RL_l is the road length of segment l; and EF_{hkt} is the emission factor of pollutant t for vehicle class k at hour h. K, L and H refer to the sets of all vehicle classes, all road segments in Hong Kong, and the study period (between 7:00 a.m. and 11:00 p.m.), respectively.

To ensure comparability across road segments of varying lengths, emissions were subsequently normalized using length- and area-based metrics for different analytical purposes. For regional and spatial analyses, total road-segment emissions were aggregated over the 16 h study period and normalized by road length (g/km) to remove biases associated with heterogeneous road lengths. For temporal analysis, emission intensity was retained at the hourly level and also reported as network-average emissions per km. Since total road length is constant across hours and vehicle classes, this normalization preserves temporal emission patterns across different vehicle classes. For the disparity analysis, emissions were normalized by buffer area (kg/km^2) as a proxy for potential population exposure in surrounding communities.

2.5. Emission Exposure Disparities

Previous studies have shown that local traffic emissions account for 58−81% of on-road NO_x levels in Hong Kong and that concentrations are strongly correlated with emissions within a 100 m radius.[22,72,73] Consistent with prior work using emission estimates as exposure proxies,[6] this study evaluated community-scale exposure disparities for NO_x by income and ethnicity using data from the 2021 Hong Kong Census.[52] Census tracts in Hong Kong represent the smallest commonly used spatial units with detailed socioeconomic information, with an average area of approximately 6.19 km^2, of which only 1.12 km^2 is zoned for residential and commercial use due to extensive mountainous land cover.

For each census tract, 100 m buffers were generated, and per-area NO_x emissions from individual vehicle classes were aggregated as a proxy for population exposure. To evaluate the plausibility of the emission-based exposure proxy, NO_x concentration data for 2023 were compiled from roadside monitoring locations in Hong Kong and aggregated to the hourly level. These hourly concentrations were compared with the area-normalized NO_x emission proxy within 100 m buffers around each monitoring site during the study hours (see details in Supporting Information). The proxy shows reasonable agreement with observed concentrations (Pearson r = 0.60; Figure S7), supporting its application as an indicator of near-road exposure variability.

Hereafter, exposure refers to area-normalized emission level (kg/km^2) within 100 m residential buffers, used as a proxy for population exposure related to near-road traffic emissions. These tract-level exposure estimates were then assigned to all residents within each census tract, such that exposure comparisons were population-weighted averages.

Mobility-weighted exposures were not estimated because the Hong Kong Travel Characteristics Survey,[42] last conducted in 2011, is outdated and lacks the spatial and demographic detail needed for this analysis. Moreover, previous studies have found strong correlations between population-based and mobility-weighted exposure estimates in cities,[74,75] suggesting that census-based analysis provides a reliable representation of exposure disparities.

Both income and ethnicity were analyzed to assess the environmental justice dimensions of exposure disparities in Hong Kong, where income polarization ranks among the highest globally, and ethnic inequalities have received limited attention in Asian environmental justice research. Monthly household income (in HKD) was classified into six categories (<$10k; $10k−20k; $20k−30k; $30k−40k; $40k−60k; ≥$60). Ethnic groups were defined as Hong Kong Chinese, Mainland Chinese, and foreign residents, with the latter further divided into White, Filipino, and Indonesian populations, the last two primarily representing domestic workers. The population of Hong Kong is composed of approximately 67.71% Hong Kong Chinese, 29.86% of Mainland Chinese, 1.92% of Filipinos, 2.72% of Indonesians, and 0.91% of White. The spatial distributions of population density by income and ethnicity are shown in Figures S8 and S9.

https://doi.org/10.1021/acs.est.5c14619
Environ. Sci. Technol. XXXX, XXX, XXX−XXX

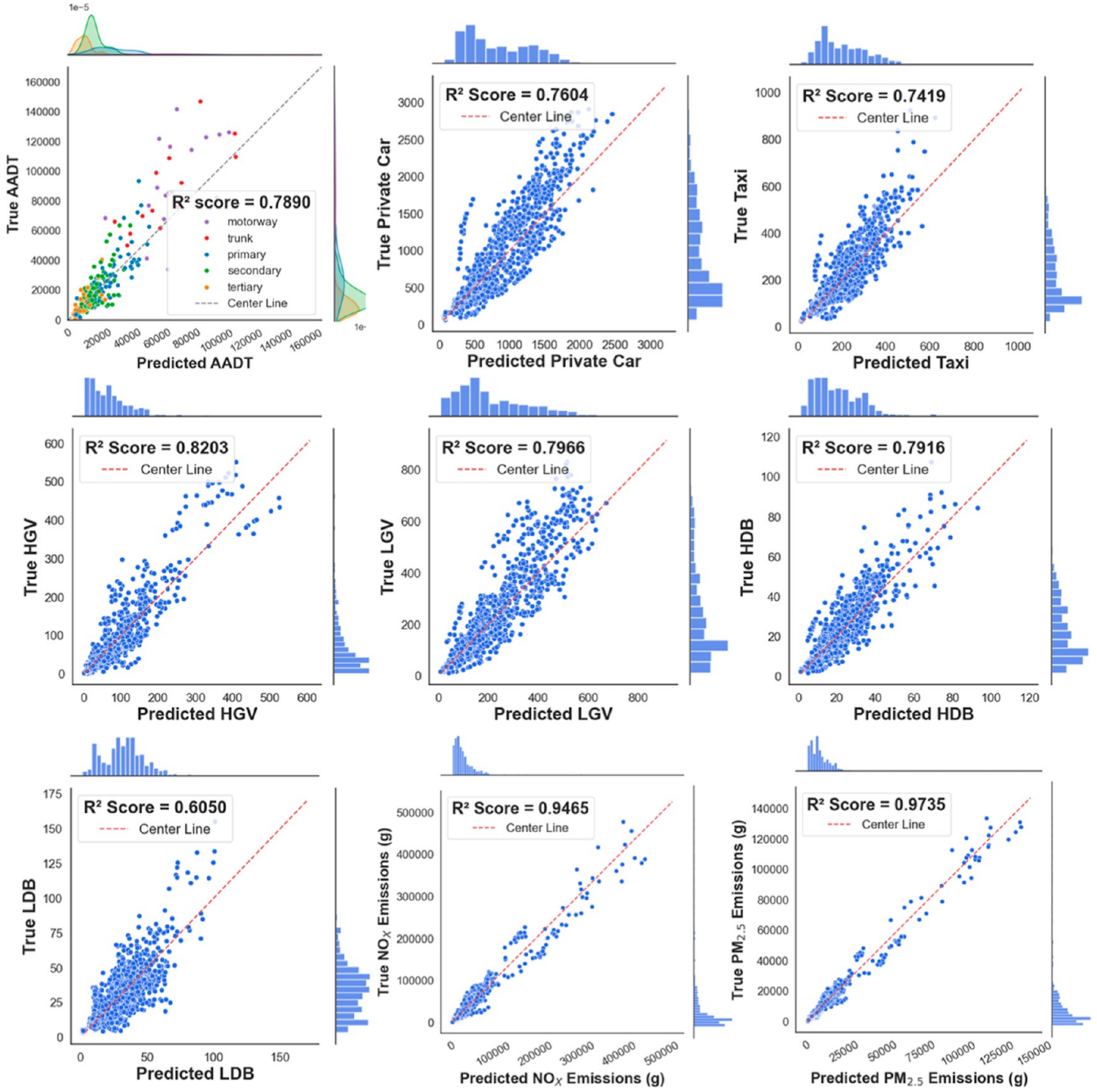

Figure 2. Comparison between predicted and observed values for (from top left to bottom right): annual average daily traffic (AADT); hourly volumes of private cars, taxis, heavy goods vehicles (HGV), light goods vehicles (LGV), heavy-duty buses (HDB), and light-duty buses (LDB); and hourly emissions of NO_x and $PM_{2.5}$. Each subplot shows the coefficient of determination (R^2) and a one-to-one reference line representing perfect agreement.

Two-sample t tests were used to assess whether differences in average population-weighted exposure between any two groups were statistically significant.[76] Mann−Whitney U tests were used to assess whether the distribution of population-weighted exposure in one group was higher than that in another group.[77]

Emission exposure disparities were expressed as the percentage difference in emissions between groups for each metric[78] using eq 2

$$D_{i,j} = \frac{E_i - E_j}{E_j} \times 100\%, \qquad \forall\, i, j \in G \tag{2}$$

where $D_{i,j}$ represents the disparity between group i and j, E_i is the average per area emissions for group i, and G refers to the set of all groups (income or ethnicity). When disparities are observed, the contribution of each vehicle class was quantified by dividing its between-group exposure disparity by the total disparity using eq 3

$$C_{i,j}^{k} = \frac{D_{i,j}^{k}}{D_{i,j}} \times 100\%, \qquad \forall\, i, j \in G, \forall\, k \in K \tag{3}$$

where $C_{i,j}^{k}$ represents the % contribution of vehicle class k to the total disparity between groups i and j, and $D_{i,j}^{k}$ denotes the exposure disparity attributable specifically to emissions from vehicle class k, and K denotes the set of vehicle classes. To capture temporal dynamics, the analysis was repeated across six time periods: early morning (7:00−8:00 a.m.), morning (8:00−10:00 a.m.), midday (10:00 a.m. to 4:00 p.m.), afternoon (4:00−5:00 p.m.), evening (5:00−7:00 p.m.),

https://doi.org/10.1021/acs.est.5c14619
Environ. Sci. Technol. XXXX, XXX, XXX−XXX

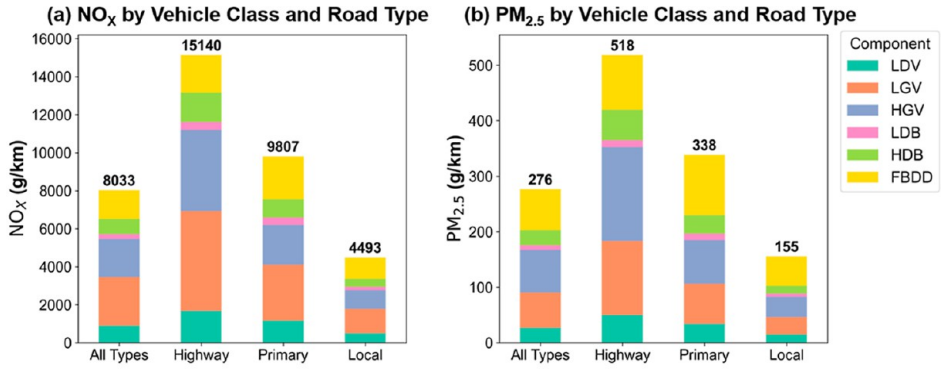

	LDV	LGV	HGV	LDB	HDB	FBDD
All Types	11%	32%	25%	3%	10%	19%
Highway	11%	35%	28%	3%	10%	13%
Primary	12%	30%	21%	4%	10%	23%
Local	11%	28%	22%	4%	9%	25%

	LDV	LGV	HGV	LDB	HDB	FBDD
All Types	10%	23%	28%	3%	10%	27%
Highway	10%	26%	33%	2%	11%	19%
Primary	10%	21%	23%	4%	10%	32%
Local	10%	20%	23%	4%	9%	34%

Figure 3. NO_x (a) and $PM_{2.5}$ (b) emissions (g/km) by vehicle class and road type. Bars represent average emissions for all roads, highways, primary roads, and local roads, with total emissions labeled above each bar and percentage contributions by vehicle class summarized below.

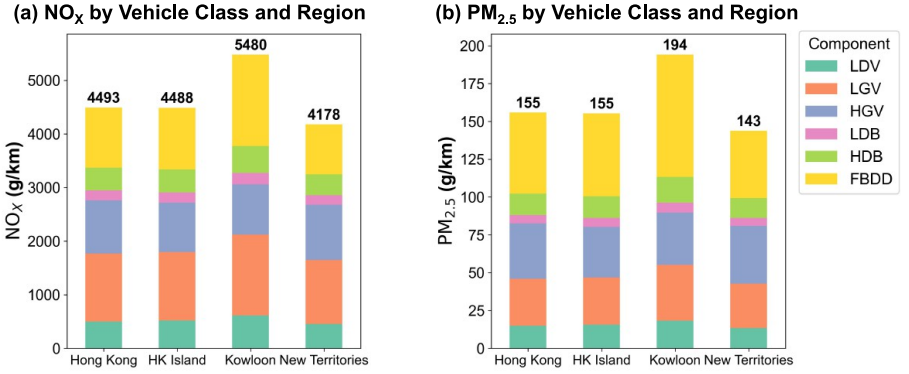

	LDV	LGV	HGV	LDB	HDB	FBDD
Hong Kong	11%	28%	22%	4%	9%	25%
HK Island	12%	28%	20%	4%	10%	26%
Kowloon	11%	28%	17%	4%	9%	31%
New Territories	11%	29%	25%	4%	9%	22%

	LDV	LGV	HGV	LDB	HDB	FBDD
Hong Kong	10%	20%	23%	4%	9%	34%
HK Island	10%	20%	22%	4%	9%	35%
Kowloon	9%	19%	18%	3%	9%	42%
New Territories	9%	20%	27%	4%	9%	31%

Figure 4. Regional distributions of (a) NO_x and (b) $PM_{2.5}$ emissions (g/km) on local roads by vehicle class. Bars represent average emissions across Hong Kong Island, Kowloon, and the New Territories, with total emissions labeled above each bar and percentage contributions summarized below.

and after-evening (7:00−11:00 p.m.). These intervals were determined because the hourly traffic patterns within each time period are similar.

3. RESULTS

3.1. Model Performance

Figure 2 shows comparisons between observed and estimated values for AADT, hourly vehicle class volumes, and hourly NO_x and $PM_{2.5}$ emissions. The XGBoost models exhibited strong performance, explaining 74.2−82.0% of the hourly volume variance across six vehicle classes. The only exception was light-duty buses (LDB), which achieved an R^2 of 0.61, indicating lower explained variability compared to other vehicle classes. Consistent with this, LDB also exhibited larger prediction errors, as reflected by higher MAPE values, reported in Table S6.

This weaker performance likely reflects the heterogeneous nature of the LDB category, which combines both public light buses (PLBs) and private minibuses. Since PLBs operate on fixed routes and schedules like FBDDs, their variability is less well captured by the model predictors. The results of the sensitivity tests assessing the influence of replacing estimated FBDD volumes with GTFS-derived volumes are summarized in Table S7. The tests show only a minor influence on the estimated volume for remaining vehicle classes.

As a second-stage validation, model-predicted emissions were compared with ground-truth values derived from observed traffic volumes and speeds by vehicle class. This comparison is to evaluate whether uncertainties in the multistage modeling propagate into the emission estimates, rather than to validate the estimates against direct measurements. The testing set achieved R^2 values of 0.95 for hourly NO_x and 0.97 for hourly $PM_{2.5}$, confirming the model's ability to capture spatiotemporal emission patterns.

The strong agreement in emissions partly reflects the accuracy of the underlying traffic-activity estimates and the detailed reconstruction of FBDD dispatches. In particular, FBDD volumes were derived from GTFS-based route reconstruction and were applied consistently in both the "ground-truth" emissions calculation and the model-based estimates. Because FBDDs account for a substantial share of total emissions, this consistency reduces discrepancies in the emission comparison. In addition, the second-stage validation subset was restricted to road segments with ground-truth

https://doi.org/10.1021/acs.est.5c14619
Environ. Sci. Technol. XXXX, XXX, XXX−XXX

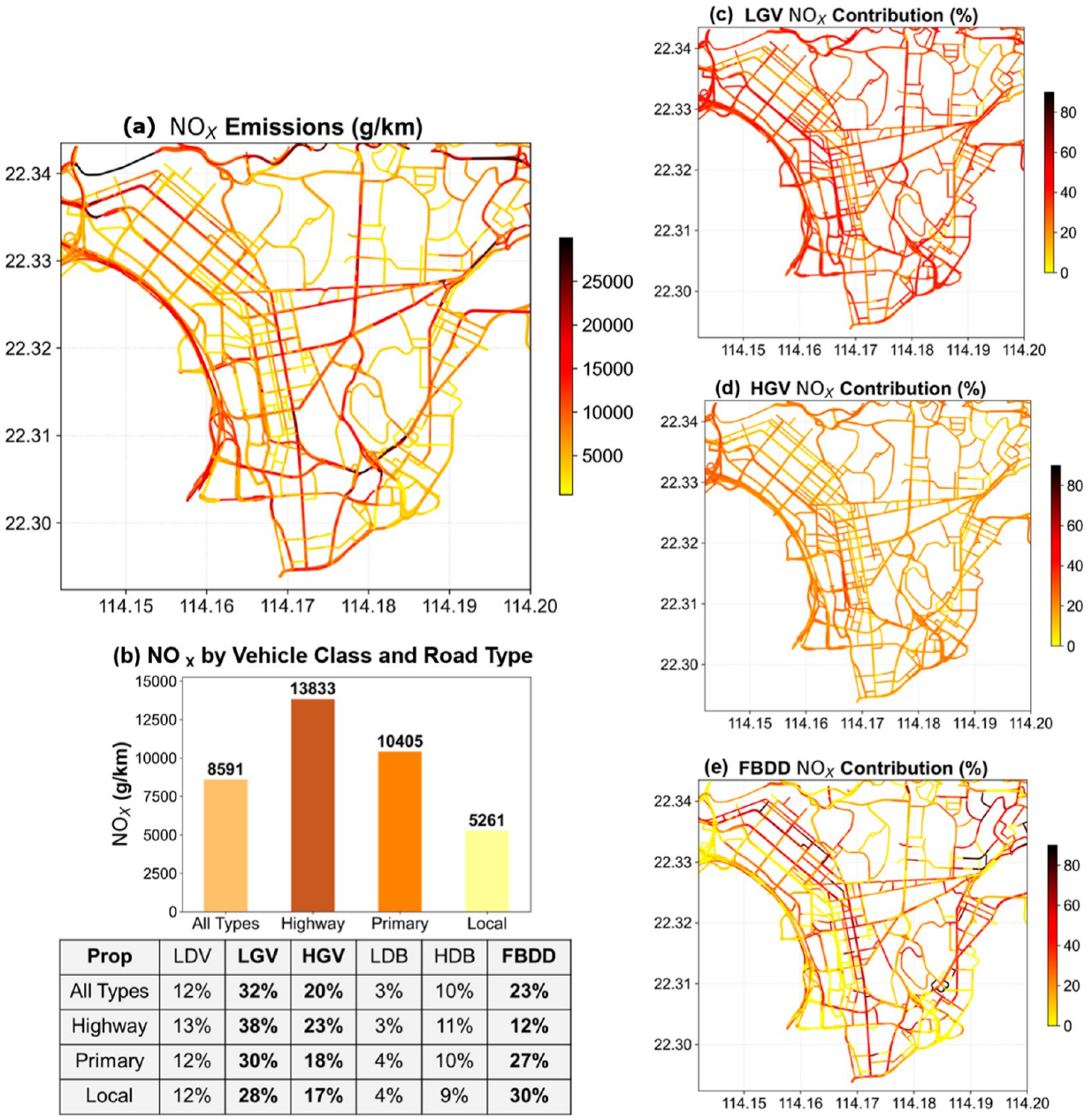

Prop	LDV	LGV	HGV	LDB	HDB	FBDD
All Types	12%	**32%**	**20%**	3%	10%	**23%**
Highway	13%	**38%**	**23%**	3%	11%	**12%**
Primary	12%	**30%**	**18%**	4%	10%	**27%**
Local	12%	**28%**	**17%**	4%	9%	**30%**

Figure 5. Spatial distribution of daily NO_x emissions (g/km) and vehicle-class contributions. (a) Road-segment level NO_x emissions; (b) average NO_x emissions and vehicle-class contributions across road types; (c−e) spatial distributions of NO_x contributions (%) from LGVs (c), HGVs (d), and FBDDs (e).

observations for all traffic variables, which increases the representation of monitored highways and may contribute to the higher R^2 for emissions. Full evaluation metrics, including R^2, RMSE, MAE, and MAPE, for all estimates are summarized in Table S6.

3.2. Regional Fleet Composition and Emission Characteristics

In this section, we calculated the length-normalized emission intensity (g/km) for each road type (Figure 3) and for each region (Figure 4) by aggregating total emissions over the 16 h study window and dividing by total road length. The emission contribution of each vehicle class was quantified by dividing the class-specific average emission by the total average emission. We grouped LDV categories, including motorcycles, private cars, and taxis, together because they contribute relatively little to total emissions. Although LDVs account for 72−74% of traffic volume across highways, primary roads, and local streets, they generate less than 12% of total NO_x and 10% of $PM_{2.5}$ emissions (Figure 3). This contrast reflects fuel differences, as most motorcycles and passenger cars are powered by gasoline, while taxis use liquefied petroleum gas, both having substantially lower emission factors than the diesel used by goods vehicles and buses.

LGVs represent the second-largest share of traffic, ranging from 14 to 16%. LGVs, HGVs, and FBDDs are the dominant emission sources across all road types, together responsible for 76% of NO_x and 78% of $PM_{2.5}$ emissions. On highways, LGVs and HGVs produce more than half of total emissions, reflecting intensive freight and logistics activities along major corridors. On local roads, FBDDs are the largest $PM_{2.5}$ emitter (34%)

https://doi.org/10.1021/acs.est.5c14619
Environ. Sci. Technol. XXXX, XXX, XXX−XXX

and the second-largest NO_x emitter (25%). Because local roads are closely connected to residential and commercial areas with high pedestrian activity, emissions from these corridors have significant implications for population exposure.

While emissions were estimated for the entire Hong Kong road network, we focused our analysis on Hong Kong Island, Kowloon, and the New Territories, which together account for all of the city's population and traffic activity and represent distinct land-use and mobility patterns. These regions were selected to examine vehicle-class emission contributions on local roads most relevant to community exposure (Figure 4).

LGVs, HGVs, and FBDDs consistently remained the dominant emission sources, although their relative importance varied across regions. On Hong Kong Island, emission patterns were broadly similar to the citywide average. In Kowloon, the most densely populated part of Hong Kong, local-road emissions were 22% higher for NO_x and 24% higher for $PM_{2.5}$ than the citywide averages. Franchised buses accounted for the largest shares of NO_x (31%) and $PM_{2.5}$ (42%) emissions, exceeding the citywide averages of 24% and 21%, respectively. These elevated levels reflect Kowloon's high residential density of about 47,600 persons per km^2, about 1.7 times that of Manhattan.[79] In contrast, HGVs contributed more in the New Territories, where highway corridors and freight routes connecting to Mainland China lead to intensive truck activity.

3.3. Spatiotemporal Dynamics of Emissions

3.3.1. Spatial Heterogeneity of Traffic Emissions. To reveal how traffic emissions vary across densely populated and socially vulnerable areas, we examined the spatial distribution of NO_x emissions within a core region of Kowloon (Figure S10). This area was selected to show neighborhood-scale patterns relevant to environmental justice, as it combines extreme population density with distinct income inequality. The region includes Mong Kok, one of the most crowded urban districts globally,[80] and Sham Shui Po, Hong Kong's lowest-income district,[52] making it an ideal setting for assessing localized exposure disparities. Spatial patterns are characterized using length-normalized emission intensity, aggregated over the 16 h study window, to highlight heterogeneity in emission intensity across the road network.

Figure 5 presents the spatial distribution of NO_x emissions and the percentage contributions of the three dominant sources, namely LGVs, HGVs, and FBDDs. Figure S11 provides the corresponding $PM_{2.5}$ map, and Figure S12 shows a map of road types for reference. Highways and primary roads (Figure 5a,b) exhibit substantially higher NO_x emission intensities, averaging 13,833 and 10,405 g/km, respectively, which are 2.6 and 2.0 times greater than those on local roads. On highways, LGVs and HGVs contribute 38% and 23% of total NO_x, while FBDDs account for only 12%, which is even lower than the share from LDVs.

In contrast, FBDDs are a major source of NO_x emissions on local roads, contributing an average of 30% of total NO_x. On some streets within densely populated residential areas, their share exceeds 80% (shown in black in Figure 5e). These local corridors are heavily used by pedestrians due to nearby housing density and close access to public transport stations, leading to elevated daily exposure to FBDD emissions. At the same time, FBDD routes provide essential mobility services, particularly for transit-dependent and lower-income communities. The observed pattern therefore reflects a trade-off between mobility provision and near-road emissions, underscoring the importance of cleaner bus technologies that can preserve service accessibility while reducing exposure burdens.

The high contribution of FBDDs to emissions on local roads reflects the structure of Hong Kong's transit system and the operational characteristics of its bus network.[81] For short intradistrict trips, travelers often prefer FBDDs because the network provides closely spaced stops and requires few transfers, resulting in higher vehicle activity and emissions on local roads. For interdistrict travel, however, frequent stops and congestion reduce bus efficiency, making the metro the preferred mode.[82] This distinction between short- and long-distance travel explains the contrasting FBDD emission levels observed across different road types.

3.3.2. Diurnal Profiles and Peak-Period Dynamics. Figure 6 shows the average hourly NO_x and $PM_{2.5}$ emissions

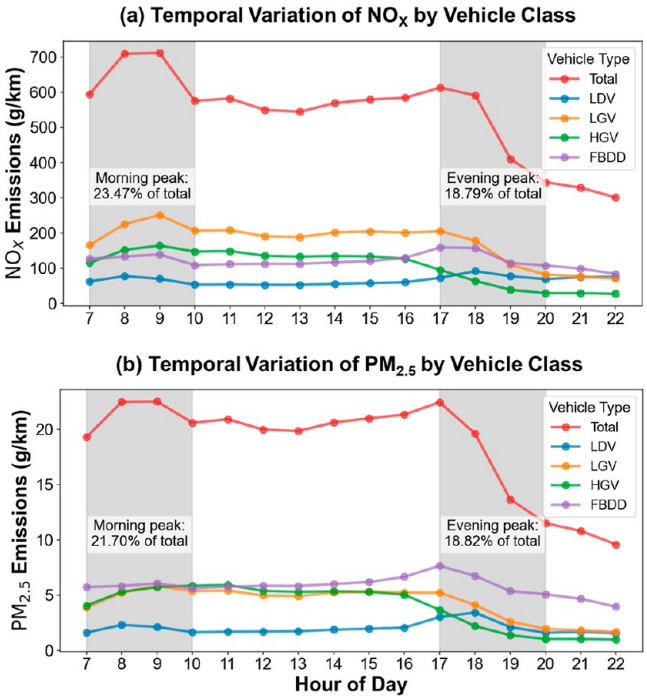

Figure 6. Hourly average emissions (g/km) of NO_x (a) and $PM_{2.5}$ (b) from total traffic and individual vehicle classes (LDVs, LGVs, HGVs, and FBDDs) in the core region of Kowloon. Morning and evening peak periods are highlighted, with respective contributions to total emissions indicated.

from total traffic and four vehicle classes (LDVs, LGVs, HGVs, and FBDDs) within the core region of Kowloon. Hourly emissions are presented as network-average emission intensity, obtained by dividing total hourly emissions by total road length. Emissions peak during the morning rush (7:00−10:00 a.m.), reaching 25% and 16% above the 16 h daytime average for NO_x and $PM_{2.5}$, respectively. In contrast, the evening peak (5:00−8:00 p.m.) shows no comparable surge, with emissions 20% and 13% lower than those in the morning peak. Across the entire Hong Kong road network (Figures S13 and S14), this contrast becomes even more distinct, as morning peaks exceed evening levels by 42% for NO_x and 32% for $PM_{2.5}$, despite total traffic volume during the morning period being 5% lower.

During the morning peak, all vehicle categories show increased activity and emissions. Commuter travel before

https://doi.org/10.1021/acs.est.5c14619
Environ. Sci. Technol. XXXX, XXX, XXX−XXX

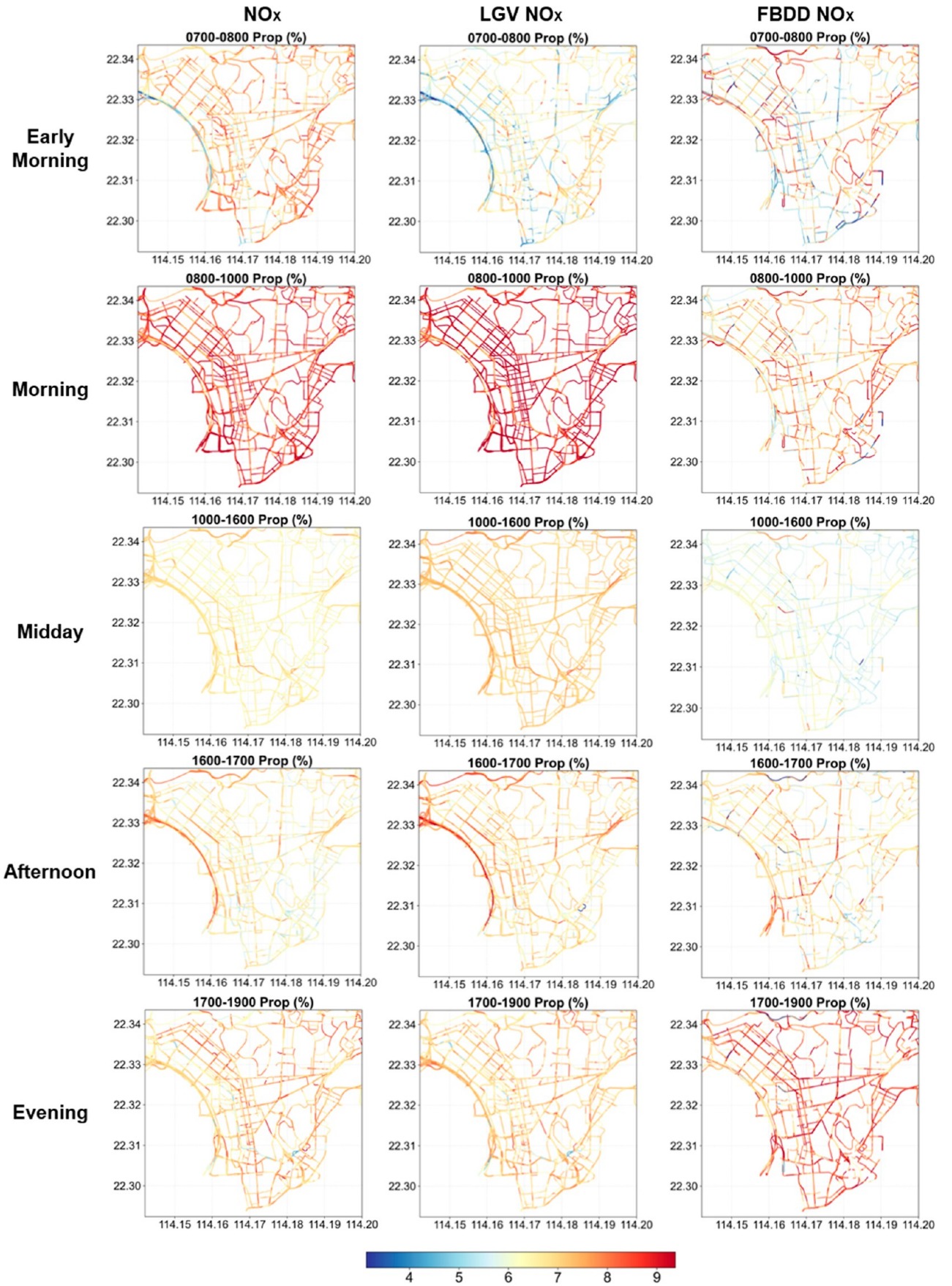

Figure 7. Spatial patterns of the proportions of average hourly NO_x emissions (1st column), LGV NO_x emissions (2nd column), and FBDD NO_x emissions (3rd column) across five time periods (corresponding to the five rows). For each road segment, the emission proportion is defined as the percentage of the average hourly emission during a given period relative to the total 16 h emission for that segment.

https://doi.org/10.1021/acs.est.5c14619
Environ. Sci. Technol. XXXX, XXX, XXX−XXX

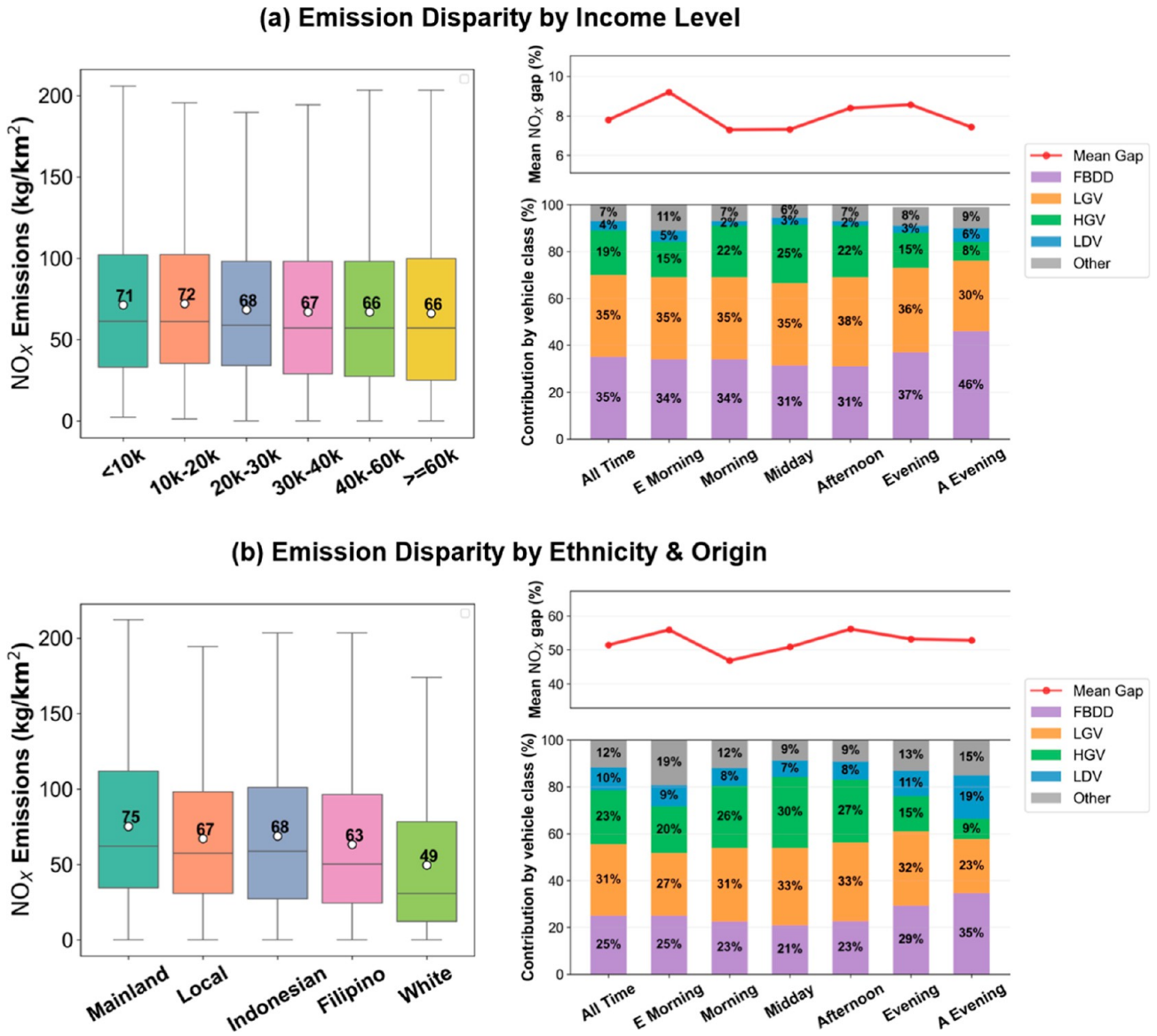

Figure 8. Distributions of NO_x emission per area by (a) income and (b) ethnic origin (Mainland = residents born in Mainland China; Local = Hong Kong-born Chinese). Boxplots in the left panels summarize group-level exposure distributions (box = interquartile range, central line = median, whiskers = values within 1.5× interquartile range, points beyond whiskers = outliers; white dot = mean). Gap decomposition plots in the right panels are shown as two stacked subplots for clarity: the upper line plot reports the mean total NO_x exposure gap (percentage difference) between the most and least advantaged groups for each time period, and the lower stacked bar plot partitions this mean total gap into the percentage contributions of each vehicle class (summing to 100%). Income groups are categorized by monthly household income in Hong Kong dollars (HKD). "All Time" represents the full 16 h study period (7 a.m. to 11 p.m.). Time periods are E morning = early morning (7−8 a.m.), morning (8−10 a.m.), midday (10 a.m. to 4 p.m.), afternoon (4−5 p.m.), evening (5−7 p.m.), and A evening = after evening (7−11 p.m.).

9:00 a.m. leads to increases in LDV and FBDD activity, while the start of commercial operations around 10:00 a.m. increases delivery traffic from LGVs and HGVs. In the evening, LDV and FBDD emissions exceed their morning levels, but LGV and HGV emissions begin to decline after 4:00 p.m. and 5:00 p.m., decreasing by 48% and 79%, respectively, by 7:00 p.m. Although LGVs and HGVs make up a smaller share of total traffic, they account for about half of total NO_x emissions. Their early decline, therefore, explains the substantial reduction in evening NO_x levels, despite total traffic volume during the evening peak being higher than that during the morning peak (Figure S14).

3.3.3. Network-Level Spatiotemporal Patterns of Emissions. To characterize spatiotemporal emission patterns, we normalized each road segment's hourly emission intensity by its total emission intensity over the 16 h study window (Figure 7). We then grouped hours into five time periods, as shown in Figure 7, because traffic activity was similar within each period. The after-evening peak period is excluded due to its low levels. For each road segment, the emission proportion represents the share of hourly average emissions that occurred during each period in the total 16 h emissions. Higher values (shown in warmer colors) indicate periods with more intense emission activity. A value of 6.25% corresponds to one-sixteenth of total emissions per hour and serves as a reference for an even temporal distribution, providing a baseline for comparison across time periods. Hourly maps of NOs_x and $PM_{2.5}$ emissions from LGVs and FBDDs are provided in

https://doi.org/10.1021/acs.est.5c14619
Environ. Sci. Technol. XXXX, XXX, XXX−XXX

Figures S15−S20, while HGVs are not shown here because their spatial pattern closely follows that of LGVs.

During the early morning period, NO_x emissions are moderate relative to the 16 h average but already elevated along many primary and local roads, primarily due to FBDDs, whose emissions exceed the average by more than 50%. LGV contributions remain comparatively low, particularly on highways where emissions are 20−70% below the average. During the morning peak, NO_x levels reach their daily maximum, with most roads exceeding 150% of the average except for a few highway segments. The spatial distribution of LGV emissions closely follows that of total NO_x, whereas FBDD emissions remain high along primary and local roads, similar to their early morning pattern. These patterns indicate that LGV activity peaks around 8:00 a.m. and lasts for about 2 h, contributing significantly to total NO_x emissions.

During the midday period, NO_x emissions remain slightly above the 16 h average across most roads, although some highways show higher values driven by continuous LGV activity throughout the region. As travel demand decreases, FBDD emissions return to near-average levels. In the early afternoon peak, NO_x levels on several highways rise to nearly 50% above average, reflecting end-of-work trips by LGVs. The evening peak shows reduced highway NO_x but elevated emissions along primary and local roads, primarily associated with FBDD operations. After 8:00 p.m. (Figures S15−S20), LGV emissions decrease to less than half of the daily average across all road types, while FBDD levels remain relatively high.

Overall, when LGV activity is minimal (before 8:00 a.m. and after 6:00 p.m.), FBDDs dominate the spatial distribution of NO_x emissions. During the active daytime period, LGVs and HGVs become the primary contributors, shaping the citywide emission pattern.

3.4. Disparities in Emission Exposure Across Socioeconomic and Ethnic Groups

To assess the distributional impacts of traffic emissions, we quantified population exposure proxies based on area-normalized NO_x levels across income and ethnic groups to examine socioeconomic disparities (Figure 8). The left panels of Figure 8a,b show that low-income residents generally experience higher NO_x emission levels than wealthier residents. The lowest-income group (<HKD 10k/month) has an 8% higher average NO_x level than the highest-income group (≥HKD 60k/month), and this difference is statistically significant in the t test (T = 50.43, p < 0.01). The most affected households, those earning HKD 10k−20k/month, have an average NO_x level 9% higher than the wealthiest group (T = 62.21, p < 0.01). The nonparametric Mann−Whitney U test was also applied to assess whether the exposure distribution in one group is generally higher than that in the comparison group. Results from the Mann−Whitney U are also significant for both comparisons (p < 0.01). These results suggest that traffic-related emissions disproportionately affect socioeconomically disadvantaged populations.

NO_x emission levels also vary significantly across ethnic and origin groups. Hong Kong-born Chinese and Mainland Chinese populations experience higher average near-road NO_x emission levels than White residents. Mainland Chinese residents are exposed to 52% higher levels (T = 126.67, p < 0.01), while Hong Kong locals face 40% higher levels (T = 98.98, p < 0.01). The average NO_x emission levels among Indonesian and Filipino populations fall between those observed for Chinese and White residents, reflecting their concentration as live-in domestic workers residing primarily in employer houses. These findings indicate that Chinese and low-income populations bear a disproportionate burden of traffic-related NO_x exposure, which may contribute to elevated health risks.

The right panels of Figure 8a,b show how average emission disparities between the most and least advantaged groups vary throughout the day and how different vehicle classes contribute to these gaps. Among income groups, LGVs (35%), FBDDs (35%), and HGVs (19%) are the dominant contributors. Disparities peak during the early morning and evening rush hours, when the FBDD contribution rises to 37%. After the evening rush hours, FBDDs account for up to 46% of the disparity. LGV and HGV contributions remain relatively high during the morning, midday, and afternoon periods.

Across ethnic groups, similar diurnal patterns are observed, though disparities narrow during the morning rush hours. LGVs account for the largest share of the exposure gap between Mainland Chinese and White populations (31%), followed by FBDDs (25%) and HGVs (23%). Compared with income disparities, ethnic disparities are less influenced by FBDDs and show a more consistent contribution from goods vehicles during daytime hours.

Together, these temporal and vehicle-type patterns highlight unequal near-road NO_x emission burdens across population groups. FBDDs generate higher emissions in low-income and Chinese neighborhoods because these populations rely heavily on public transit, leading to denser bus routes and more frequent services. At the same time, these services provide essential mobility and accessibility benefits for these transit-dependent communities. LGVs also contribute substantially to disparities due to the spatial clustering of freight activity and its daytime intensity. These findings highlight the need for vehicle- and time-specific mitigation measures to reduce disproportionate exposure burdens among disadvantaged communities.

4. DISCUSSION

4.1. Advancing Traffic-Emission Modeling for High-Resolution Urban Analysis

This study introduces a data-driven framework that integrates machine learning and deep learning models to estimate hourly traffic volumes and emissions for eight vehicle classes across Hong Kong's road network. Each modeling step, from AADT inputs to hourly emissions, was validated using multiple data sources, resulting in strong predictive performance. The model explains about 74−82% of the variation in hourly traffic volumes across most vehicle classes and approximately 95% of the variation in hourly NO_x and $PM_{2.5}$ emissions compared with observed data. Given that previous studies in Hong Kong have documented large traffic-related pollutant gradients over short distances and time periods,[13,18] the high spatially and temporally resolved traffic emissions generated by our model can reveal localized exposure hotspots in dense urban environments.

The framework provides a replicable and adaptable workflow that can be continuously updated using open traffic data sets, offering a scalable and continuously improving alternative to traditional travel surveys that are conducted only every five to ten years.[8,24] This dynamic capability allows near-real-time

https://doi.org/10.1021/acs.est.5c14619
Environ. Sci. Technol. XXXX, XXX, XXX−XXX

evaluation of emission trends and exposure inequalities under rapidly evolving fleet compositions and urban policy scenarios.

While the framework shows strong predictive capability, further refinements could enhance its robustness. The accuracy of AADT estimates and vehicle detection remains sensitive to image quality, camera placement, and spatial coverage, leading to uncertainty in under-monitored corridors. Integrating field measurements, telematics, and roadside pollution data could improve calibration accuracy and reduce spatial bias. Future mobile monitoring campaigns would provide valuable data for calibration and validation of emission-based exposure estimates.

4.2. Interpreting Spatiotemporal Emission Patterns and Exposure Inequities

The class-resolved results reveal that LGVs, HGVs, and FBDDs together account for more than three-quarters of total on-road NO_x and $PM_{2.5}$ emissions. While LGVs and HGVs dominate emissions on highways, FBDDs contribute the most along local roads where pedestrian exposure is highest. As elevated vehicular emissions have been linked to adverse health outcomes in a district-level analysis of Hong Kong,[12] the disproportionate contribution of buses to emissions on densely populated local roads highlights the need for targeted emission reductions for buses to mitigate health impacts. These results support recent transport decarbonization strategies prioritizing bus electrification in dense neighborhoods.[83]

Temporal patterns further indicate that morning emission peaks are driven by concurrent commuter and freight activities, whereas evening peaks are dominated by public transit operations. This temporal asymmetry underscores how distinct vehicle classes shape the temporal dynamics of near-road emission burdens across the day. Although freight restrictions have shifted goods vehicle activity to nighttime hours in some cities,[84,85] Hong Kong's pattern remains daytime-concentrated, increasing potential exposure in mixed-use corridors adjacent to housing. A dispersion-based study has confirmed this high exposure risk in Hong Kong by showing that residents near major roadways experience disproportionately higher exposure to vehicular pollutants.[14]

The socioeconomic and ethnic analyses show clear inequalities in near-road NO_x emission burdens. Low-income residents experience, on average, 8−9% higher near-road NO_x emission levels than wealthier residents, while Mainland Chinese and Hong Kong locals experience 40−52% higher levels compared with White residents. These gaps are comparable in magnitude to racial disparities reported in North American studies,[5,6,8,23] confirming that transport-related environmental inequality extends to Asian cities. Importantly, epidemiological evidence in Hong Kong also indicates that lower socioeconomic groups experience greater mortality risks associated with traffic-related air pollutants,[12] suggesting that observed exposure disparities translate into health inequities. These disparities reflect spatially structured inequities in near-road emission burdens linked to residential location and socioeconomic position, rather than causal effects of ethnic identity.

4.3. Policy and Planning Implications for Equitable Emission Reduction

Disparities vary throughout the day, peaking during the morning and evening rush hours and declining at midday. LGVs and FBDDs are the largest contributors to emission-burden gaps, together explaining more than half of the observed differences. LGV- and HGV-related disparities intensify during daytime freight activity, whereas bus-related disparities are most prominent in the evening. Compared with income-based differences, ethnic disparities show a smaller influence from FBDDs and steadier contributions from goods vehicles during daytime hours.

These patterns point to structural causes rooted in land-use configurations. Public housing estates and working-class neighborhoods experience denser bus routes and higher service frequencies, while freight activities concentrate near older urban cores with limited street ventilation and green buffers. Mitigation should therefore be targeted by both fleet type and time of day. Electrifying franchised buses along routes serving disadvantaged areas and incentivizing LGV electrification can substantially reduce disparities. Beyond vehicle electrification, optimizing bus operations, such as route design and short-run strategies,[86] may help reduce emissions while maintaining accessibility. For freight transport, measures such as eco-routing and targeted low-emission zones that discourage high-emitting vehicles from operating in densely populated areas could also alleviate near-road emission burdens for vulnerable populations.[87,88]

Looking ahead, the emission-based framework offers a practical and policy-relevant proxy for identifying environmental inequality. Future work could build upon this foundation by linking emissions with dispersion or exposure models to explore health implications and cumulative risks. Such integration would broaden the framework's utility for evaluating mitigation strategies while maintaining its strength in revealing structural sources of transport-related inequality in dense urban environments.

4.4. Limitations

While this study provides a high-resolution assessment of traffic emissions and emission-based exposure proxies, it does not account for meteorological processes or atmospheric chemistry that govern pollutant dispersion and transformation. In addition, the linkage between on-road emissions and residential exposure may be attenuated by the city's distinctive vertical urban form. As one of the highest-density high-rise cities globally, Hong Kong exhibits strong vertical gradients in dilution, dispersion, and building ventilation, which may reduce exposure for residents living at higher elevations. This vertical attenuation introduces additional uncertainty when using street-level emissions and horizontal proximity alone as proxies for population exposure.

Beyond on-road traffic, Hong Kong's ambient air quality is also influenced by regional transport and secondary formation. Source apportionment and chemical transport modeling studies have shown that seasonal $PM_{2.5}$ can be strongly affected by cross-boundary inflow from the Pearl River Delta and broader South China.[89,90] Our analysis focuses on primary traffic emissions that capture near-road spatial variability, but it does not quantify the relative contributions of regional background pollution versus local sources to ambient concentrations. Accordingly, our results should be interpreted as indicators of near-road, traffic-driven inequities rather than a comprehensive attribution of territory-wide air pollution disparities.

Another limitation is the use of a cycle-calibrated emission factor model to estimate emissions on road segments that represent only portions of complete trip cycles. Link-level average-speed inputs are not fully consistent with the trip-

https://doi.org/10.1021/acs.est.5c14619
Environ. Sci. Technol. XXXX, XXX, XXX−XXX

based driving cycles used to calibrate EMFAC-HK, which may introduce additional uncertainty in microscale emission estimates for short urban segments. The broader emissions modeling literature indicates that average-speed methods can bias link-level emissions relative to trajectory-based or operating-mode methods.[91,92] For example, corrected average-speed frameworks have shown that conventional average-speed estimates can underpredict link-level CO_2 emissions by roughly 9−14% compared with second-by-second trajectory data on urban roads.[91] While our link-level average-speed inputs differ from the trip-based driving cycles used to calibrate EMFAC-HK, this approach enables network-wide emission estimation in the absence of continuous vehicle trajectory data. Accordingly, the results of this study are best viewed as characterizing network-scale spatiotemporal emission patterns and relative disparities across the urban road network. Future work could reduce this uncertainty by developing Hong Kong−specific correction factors using locally observed vehicle trajectories (e.g., GPS or probe data) to better represent transient driving operations while maintaining network-wide coverage.

■ ASSOCIATED CONTENT

Supporting Information

The Supporting Information is available free of charge at https://pubs.acs.org/doi/10.1021/acs.est.5c14619.

Parameter tuning and evaluation of YOLOv10-x for vehicle detection; hyperparameter tuning of XGBoost model; traffic volume adjustment; exposure proxy evaluation; supplementary figures (S1−S20); supplementary tables (S1−S7) (PDF)

■ AUTHOR INFORMATION

Corresponding Author

Junshi Xu − *Department of Geography, The Jockey Club Tower, Centennial Campus, The University of Hong Kong, Hong Kong SAR 999077, China;* orcid.org/0000-0003-2834-2291; Phone: +852 391-03254; Email: junshixu@hku.hk

Authors

Chenming Niu − *Department of Geography, The Jockey Club Tower, Centennial Campus, The University of Hong Kong, Hong Kong SAR 999077, China;* orcid.org/0009-0006-2879-6065

Qiuzi Chen − *School of Architecture, Civil and Environmental Engineering, École Polytechnique Fédérale de Lausanne (EPFL), Lausanne CH-1015, Switzerland;* orcid.org/0000-0001-9950-8274

An Wang − *Department of Civil and Environmental Engineering, The Hong Kong Polytechnic University, Hong Kong SAR 999077, China;* orcid.org/0000-0002-1874-2702

Complete contact information is available at: https://pubs.acs.org/10.1021/acs.est.5c14619

Funding

This research was supported by the Early Career Scheme (ECS) of the Research Grants Council of Hong Kong (RGC ref. No. 27608825); the National Natural Science Foundation of China (NSFC) Youth Science Fund (Type C) (Project No. 42501572); the Research Support Fund from the Department of Geography, The University of Hong Kong; the Hui Oi-Chow Trust Fund, The University of Hong Kong; and the Seed Fund for Basic Research for New Staff from the University Research Committee (URC), The University of Hong Kong.

Notes

The authors declare no competing financial interest.

■ REFERENCES

(1) Rowangould, G. M. A Census of the US Near-Roadway Population: Public Health and Environmental Justice Considerations. *Transp. Res., Part D Transp. Environ.* **2013**, *25*, 59−67.

(2) Jerrett, M. Global Geographies of Injustice in Traffic-Related Air Pollution Exposure. *Epidemiology* **2009**, *20* (2), 231−233.

(3) Miranda, M. L.; Edwards, S. E.; Keating, M. H.; Paul, C. J. Making the Environmental Justice Grade: The Relative Burden of Air Pollution Exposure in the United States. *Int. J. Environ. Res. Public Health* **2011**, *8* (6), 1755−1771.

(4) Hajat, A.; Hsia, C.; O'Neill, M. S. Socioeconomic Disparities and Air Pollution Exposure: A Global Review. *Curr. Environ. Health Rep.* **2015**, *2* (4), 440−450.

(5) Wen, Y.; Yu, Q.; He, B. Y.; Ma, J.; Zhang, S.; Wu, Y.; Zhu, Y. Persistent Environmental Injustice Due to Brake and Tire Wear Emissions and Heavy-Duty Trucks in Future California Zero-Emission Fleets. *Environ. Sci. Technol.* **2024**, *58* (43), 19372−19384.

(6) Zalzal, J.; Hatzopoulou, M. Fifteen Years of Community Exposure to Heavy-Duty Emissions: Capturing Disparities over Space and Time. *Environ. Sci. Technol.* **2022**, *56* (23), 16621−16632.

(7) Xu, J.; Saeedi, M.; Zalzal, J.; Zhang, M.; Ganji, A.; Mallinen, K.; Wang, A.; Lloyd, M.; Venuta, A.; Simon, L.; Weichenthal, S.; Hatzopoulou, M. Exploring the Triple Burden of Social Disadvantage, Mobility Poverty, and Exposure to Traffic-Related Air Pollution. *Sci. Total Environ.* **2024**, *920*, 170947.

(8) Wen, Y.; Zhang, S.; Wang, Y.; Yang, J.; He, L.; Wu, Y.; Hao, J. Dynamic Traffic Data in Machine-Learning Air Quality Mapping Improves Environmental Justice Assessment. *Environ. Sci. Technol.* **2024**, *58*, 3118.

(9) Xu, J.; Ganji, A.; Saeedi, M.; Jeong, C.-H.; Su, Y.; Munoz, T.; Lloyd, M.; Weichenthal, S.; Evans, G.; Hatzopoulou, M. Unveiling the Impact of Wildfires on Nanoparticle Characteristics and Exposure Disparities through Mobile and Fixed-Site Monitoring in Toronto, Canada. *Environ. Sci. Technol.* **2025**, *59* (11), 5621−5635.

(10) Lau, J.; Hung, W. T.; Cheung, C. S.; Yuen, D. Contributions of Roadside Vehicle Emissions to General Air Quality in Hong Kong. *Transp. Res., Part D Transp. Environ.* **2008**, *13* (1), 19−26.

(11) Barnes, J. H.; Chatterton, T. J.; Longhurst, J. W. S. Emissions vs Exposure: Increasing Injustice from Road Traffic-Related Air Pollution in the United Kingdom. *Transp. Res., Part D Transp. Environ.* **2019**, *73*, 56−66.

(12) Mak, H. W. L.; Ng, D. C. Y. Spatial and Socio-Classification of Traffic Pollutant Emissions and Associated Mortality Rates in High-Density Hong Kong via Improved Data Analytic Approaches. *Int. J. Environ. Res. Public Health* **2021**, *18* (12), 6532.

(13) Che, W.; Zhang, Y.; Lin, C.; Fung, Y. H.; Fung, J. C. H.; Lau, A. K. H. Impacts of Pollution Heterogeneity on Population Exposure in Dense Urban Areas Using Ultra-Fine Resolution Air Quality Data. *J. Environ. Sci.* **2023**, *125*, 513−523.

(14) Fan, X.; Lam, K.; Yu, Q. Differential Exposure of the Urban Population to Vehicular Air Pollution in Hong Kong. *Sci. Total Environ.* **2012**, *426*, 211−219.

(15) Wu, X.; Yang, D.; Wu, R.; Gu, J.; Wen, Y.; Zhang, S.; Wu, R.; Wang, R.; Xu, H.; Zhang, K. M.; Wu, Y.; Hao, J. High-Resolution Mapping of Regional Traffic Emissions Using Land-Use Machine Learning Models. *Atmos. Chem. Phys.* **2022**, *22* (3), 1939−1950.

(16) Li, X.; Gu, D.; Hohenberger, T. L.; Fung, Y. H.; Fung, J. C. H.; Lau, A. K. H.; Liang, Z. Dynamic Quantification of On-Road

Emissions in Hong Kong: Impact from Traffic Congestion and Fleet Composition Variation. *Atmos. Environ.* **2023**, *313*, 120059.
(17) Boikos, C.; Ioannidis, G.; Rapkos, N.; Tsegas, G.; Katsis, P.; Ntziachristos, L. Estimating Daily Road Traffic Pollution in Hong Kong Using CFD Modelling: Validation and Application. *Build. Environ.* **2025**, *267*, 112168.
(18) Zhu, Y.; Chan, K. L.; Lam, Y. F.; Horbanski, M.; Pöhler, D.; Boll, J.; Lipkowitsch, I.; Ye, S.; Wenig, M. Analysis of Spatial and Temporal Patterns of On-Road NO 2 Concentrations in Hong Kong. *Atmos. Meas. Tech.* **2018**, *11* (12), 6719−6734.
(19) Wu, L.; Chang, M.; Wang, X.; Hang, J.; Zhang, J.; Wu, L.; Shao, M. Development of the Real-Time On-Road Emission (ROE v1.0) Model for Street-Scale Air Quality Modeling Based on Dynamic Traffic Big Data. *Geosci. Model Dev.* **2020**, *13* (1), 23−40.
(20) Minet, L.; Liu, R.; Valois, M.-F.; Xu, J.; Weichenthal, S.; Hatzopoulou, M. Development and Comparison of Air Pollution Exposure Surfaces Derived from On-Road Mobile Monitoring and Short-Term Stationary Sidewalk Measurements. *Environ. Sci. Technol.* **2018**, *52* (6), 3512−3519.
(21) Wang, J. M.; Jeong, C.-H.; Hilker, N.; Shairsingh, K. K.; Healy, R. M.; Sofowote, U.; Debosz, J.; Su, Y.; McGaughey, M.; Doerksen, G.; Munoz, T.; White, L.; Herod, D.; Evans, G. J. Near-Road Air Pollutant Measurements: Accounting for Inter-Site Variability Using Emission Factors. *Environ. Sci. Technol.* **2018**, *52* (16), 9495−9504.
(22) Wei, P.; Brimblecombe, P.; Yang, F.; Anand, A.; Xing, Y.; Sun, L.; Sun, Y.; Chu, M.; Ning, Z. Determination of Local Traffic Emission and Non-Local Background Source Contribution to on-Road Air Pollution Using Fixed-Route Mobile Air Sensor Network. *Environ. Pollut.* **2021**, *290*, 118055.
(23) Yang, J.; Wen, Y.; Wang, Y.; Zhang, S.; Pinto, J. P.; Pennington, E. A.; Wang, Z.; Wu, Y.; Sander, S. P.; Jiang, J. H.; Hao, J.; Yung, Y. L.; Seinfeld, J. H. From COVID-19 to Future Electrification: Assessing Traffic Impacts on Air Quality by a Machine-Learning Model. *Proc. Natl. Acad. Sci. U. S. A.* **2021**, *118* (26), No. e2102705118.
(24) Tu, R.; Kamel, I.; Wang, A.; Abdulhai, B.; Hatzopoulou, M. Development of a Hybrid Modelling Approach for the Generation of an Urban On-Road Transportation Emission Inventory. *Transp. Res., Part D Transp. Environ.* **2018**, *62*, 604−618.
(25) Thaneya, A. B.; Horvath, A. Exploring Regional Reduction Pathways for Human Exposure to Fine Particulate Matter (PM 2.5) Using a Traffic Assignment Model. *Environ. Sci. Technol.* **2023**, *57* (48), 19649−19662.
(26) Lang, V. A.; Camilleri, S. F.; van der Lee, S.; Rowangould, G.; Antonczak, B.; Thompson, T. M.; Harris, M. H.; Harkins, C.; Tong, D. Q.; Janssen, M.; Adelman, Z. E.; Horton, D. E. Intercomparison of Modeled Urban-Scale Vehicle NO x and PM 2.5 Emissions−Implications for Equity Assessments. *Environ. Sci. Technol.* **2025**, *59* (9), 4560−4570.
(27) Wang, A.; Xu, J.; Tu, R.; Zhang, M.; Adams, M.; Hatzopoulou, M. Near-Road Air Quality Modelling That Incorporates Input Variability and Model Uncertainty. *Environ. Pollut.* **2021**, *284*, 117145.
(28) Ai, Z. T.; Mak, C. M.; Lee, H. C. Roadside Air Quality and Implications for Control Measures: A Case Study of Hong Kong. *Atmos. Environ.* **2016**, *137*, 6−16.
(29) Apte, J. S.; Messier, K. P.; Gani, S.; Brauer, M.; Kirchstetter, T. W.; Lunden, M. M.; Marshall, J. D.; Portier, C. J.; Vermeulen, R. C. H.; Hamburg, S. P. High-Resolution Air Pollution Mapping with Google Street View Cars: Exploiting Big Data. *Environ. Sci. Technol.* **2017**, *51* (12), 6999−7008.
(30) Xu, J.; Zhang, M.; Ganji, A.; Mallinen, K.; Wang, A.; Lloyd, M.; Venuta, A.; Simon, L.; Kang, J.; Gong, J.; Zamel, Y.; Weichenthal, S.; Hatzopoulou, M. Prediction of Short-Term Ultrafine Particle Exposures Using Real-Time Street-Level Images Paired with Air Quality Measurements. *Environ. Sci. Technol.* **2022**, *56* (18), 12886−12897.
(31) Wang, A.; Xu, J.; Tu, R.; Saleh, M.; Hatzopoulou, M. Potential of Machine Learning for Prediction of Traffic Related Air Pollution. *Transp. Res., Part D Transp. Environ.* **2020**, *88*, 102599.
(32) Su, J. G.; Apte, J. S.; Lipsitt, J.; Garcia-Gonzales, D. A.; Beckerman, B. S.; de Nazelle, A.; Texcalac-Sangrador, J. L.; Jerrett, M. Populations Potentially Exposed to Traffic-Related Air Pollution in Seven World Cities. *Environ. Int.* **2015**, *78*, 82−89.
(33) Kingham, S.; Pearce, J.; Zawar-Reza, P. Driven to Injustice? Environmental Justice and Vehicle Pollution in Christchurch, New Zealand. *Transp. Res., Part D Transp. Environ.* **2007**, *12* (4), 254−263.
(34) Wang, A.; Fallah-Shorshani, M.; Xu, J.; Hatzopoulou, M. Characterizing Near-Road Air Pollution Using Local-Scale Emission and Dispersion Models and Validation against in-Situ Measurements. *Atmos. Environ.* **2016**, *142*, 452−464.
(35) Gaffron, P.; Niemeier, D. School Locations and Traffic Emissions—Environmental (In)Justice Findings Using a New Screening Method. *Int. J. Environ. Res. Public Health* **2015**, *12* (2), 2009−2025.
(36) Matthias, V.; Bieser, J.; Mocanu, T.; Pregger, T.; Quante, M.; Ramacher, M. O. P.; Seum, S.; Winkler, C. Modelling Road Transport Emissions in Germany − Current Day Situation and Scenarios for 2040. *Transp. Res., Part D Transp. Environ.* **2020**, *87*, 102536.
(37) Torbatian, S.; Saleh, M.; Xu, J.; Minet, L.; Gamage, S. M.; Yazgi, D.; Yamanouchi, S.; Roorda, M. J.; Hatzopoulou, M. Societal Co-Benefits of Zero-Emission Vehicles in the Freight Industry. *Environ. Sci. Technol.* **2024**, *58* (18), 7814−7825.
(38) Heyer, J.; Palm, M.; Niemeier, D. Are We Keeping up? Accessibility, Equity and Air Quality in Regional Planning. *J. Transport Geogr.* **2020**, *89*, 102891.
(39) Bein, K. J.; Wallis, C. D.; Silverman, J. L.; Lein, P. J.; Wexler, A. S. Emulating Near-Roadway Exposure to Traffic-Related Air Pollution via Real-Time Emissions from a Major Freeway Tunnel System. *Environ. Sci. Technol.* **2022**, *56* (11), 7083−7095.
(40) Apte, J. S.; Kirchstetter, T. W.; Reich, A. H.; Deshpande, S. J.; Kaushik, G.; Chel, A.; Marshall, J. D.; Nazaroff, W. W. Concentrations of Fine, Ultrafine, and Black Carbon Particles in Auto-Rickshaws in New Delhi, India. *Atmos. Environ.* **2011**, *45* (26), 4470−4480.
(41) Batisse, E.; Lloyd, M.; Cavanaugh, A.; Ganji, A.; Xu, J.; Hatzopoulou, M.; Baumgartner, J.; Weichenthal, S. Examining the Social Distributions in Neighbourhood Black Carbon and Ultrafine Particles in Montreal and Toronto, Canada. *Environ. Int.* **2025**, *198*, 109395.
(42) TD. Travel Characteristics Survey 2011 Final Report, 2014. https://www.td.gov.hk/filemanager/en/content_4652/tcs2011_eng.pdf (accessed July 23, 2025).
(43) TD. Survey on Goods Vehicle Trip Characteristics 2011, 2014. https://www.td.gov.hk/en/publications_and_press_releases/publications/free_publications/survey_on_goods_vehicles_trip_characteristics_2011/index.html (accessed July 03, 2025).
(44) Koolik, L. H.; Alvarado, A. ·.; Budahn, A.; Plummer, L.; Marshall, J. D.; Apte, J. S. PM 2.5 Exposure Disparities Persist despite Strict Vehicle Emissions Controls in California. *Sci. Adv.* **2024**, *10* (37), No. eadn8544.
(45) Buckley, L.; Arter, C. A.; Willis, M. D.; Geddes, J. A.; Rick, C.; Kinney, P. L.; Arunachalam, S.; Buonocore, J. J.; Levy, J. I. A Comparison of Population-Level Exposure and Equity Tradeoffs across Strategies to Reduce Fine Particulate Matter Emissions from Transportation Sources in the Northeastern US. *Environ. Res.* **2024**, *262*, 119791.
(46) Pulugurtha, S. S.; Mathew, S. Modeling AADT on Local Functionally Classified Roads Using Land Use, Road Density, and Nearest Nonlocal Road Data. *J. Transport Geogr.* **2021**, *93*, 103071.
(47) Ganji, A.; Shekarrizfard, M.; Harpalani, A.; Coleman, J.; Hatzopoulou, M. Methodology for Spatio-temporal Predictions of Traffic Counts across an Urban Road Network and Generation of an On-road Greenhouse Gas Emission Inventory. *Comput. Aided Civ. Infrastruct. Eng.* **2020**, *35* (10), 1063−1084.
(48) Barmpounakis, E.; Montesinos-Ferrer, M.; Gonzales, E. J.; Geroliminis, N. Empirical Investigation of the Emission-Macroscopic Fundamental Diagram. *Transp. Res., Part D Transp. Environ.* **2021**, *101*, 103090.

https://doi.org/10.1021/acs.est.5c14619
Environ. Sci. Technol. XXXX, XXX, XXX−XXX

(49) Lloyd, M.; Ganji, A.; Xu, J.; Venuta, A.; Simon, L.; Zhang, M.; Saeedi, M.; Yamanouchi, S.; Apte, J.; Hong, K.; Hatzopoulou, M.; Weichenthal, S. Predicting Spatial Variations in Annual Average Outdoor Ultrafine Particle Concentrations in Montreal and Toronto, Canada: Integrating Land Use Regression and Deep Learning Models. *Environ. Int.* **2023**, *178*, 108106.
(50) Chen, J.; Zhu, S.; Wang, P.; Zheng, Z.; Shi, S.; Li, X.; Xu, C.; Yu, K.; Chen, R.; Kan, H.; Zhang, H.; Meng, X. Predicting Particulate Matter, Nitrogen Dioxide, and Ozone across Great Britain with High Spatiotemporal Resolution Based on Random Forest Models. *Sci. Total Environ.* **2024**, *926*, 171831.
(51) Wu, S.; Sun, D. J.; Qiu, G. Emission Analysis Based on Mixed Traffic Flow and License Plate Recognition Model. *Transp. Res., Part D Transp. Environ.* **2024**, *134*, 104331.
(52) Census and Statistics Department of HK. 2021 Population Census (Statistics and Boundaries of Small Subunit Groups). https://data.gov.hk/en-data/dataset/hk-censtatd-census_geo-2021-population-census-by-ssg (accessed Mar 03, 2025).
(53) GovHK. Public Housing and Subsidised Home Ownership Schemes. https://www.gov.hk/en/residents/housing/publichousing/index.htm (accessed Sept 15, 2025).
(54) OXFAM Hong Kong. Hong Kong Poverty Report 2024, 2024. https://www.oxfam.org.hk/en/f/news_and_publication/115439/POVERTy%20Rerport%202024_Eng.pdf (accessed July 30, 2025).
(55) Transport and Housing Bureau of Hong Kong; Transport Department of Hong Kong. Private Cars in Hong Kong, 2022. https://www.legco.gov.hk/research-publications/english/2022issh01-private-cars-in-hong-kong-20220210-e.pdf (accessed Jan 06, 2026).
(56) TD. The Annual Traffic Census 2023, 2023. https://atc.td.gov.hk/2023/AnnualTrafficCensus2023.pdf (accessed Mar 14, 2025).
(57) Environmental Protection Department of Hong Kong. 2023 Hong Kong Emission Inventory Report, 2025. https://www.epd.gov.hk/epd/sites/default/files/epd/2023_Emission_Inventory_Report_Eng_final.pdf (accessed Jan 05, 2026).
(58) TD. Traffic snapshot images. https://data.gov.hk/en-data/dataset/hk-td-tis_2-traffic-snapshot-images (accessed July 20, 2024).
(59) TD. Traffic Data of Strategic/Major Roads. https://data.gov.hk/en-data/dataset/hk-td-sm_4-traffic-data-strategic-major-roads (accessed July 15, 2025).
(60) TD. Vehicle Classification System, 2021. https://atc.td.gov.hk/pdf/2021/ATC2021-AppendixF.pdf (accessed July 16, 2024).
(61) EPD. EMFAC-HK User's Guide, 2021. https://www.epd.gov.hk/epd/sites/default/files/epd/User%20Guide%20Emfac-HK%20%28Ver%204.3%29.pdf (accessed July 17, 2024).
(62) Wang, A.; Chen, H.; Liu, L.; Chen, K.; Lin, Z.; Han, J.; Ding, G. Yolov10: Real-Time End-to-End Object Detection. *Adv. Neural Inf. Process. Syst.* **2024**, *37*, 107984−108011.
(63) Chen, T.; Guestrin, C. XGBoost: A Scalable Tree Boosting System. *Proceedings of the 22nd ACM SIGKDD International Conference on Knowledge Discovery and Data Mining*; ACM: New York, NY, USA, 2016, pp 785−794.
(64) Das, S.; Tsapakis, I. Interpretable Machine Learning Approach in Estimating Traffic Volume on Low-Volume Roadways. *Int. J. Transport. Sci. Tech.* **2020**, *9* (1), 76−88.
(65) TD. Routes and fares of public transport. https://data.gov.hk/en-data/dataset/hk-td-tis_3-routes-and-fares-of-public-transport (accessed Mar 16, 2025).
(66) Vieira, J. P. B.; Pereira, R. H. M.; Andrade, P. R. Estimating Public Transport Emissions from General Transit Feed Specification Data. *Transp. Res., Part D Transp. Environ.* **2023**, *119*, 103757.
(67) Dijkstra, E. W. A Note on Two Problems in Connexion with Graphs. In *Edsger Wybe Dijkstra*; ACM: New York, NY, USA, 2022; pp 287−290.
(68) GovHK. Monitoring Service Frequencies of Franchised Buses, 2023. https://www.info.gov.hk/gia/general/202311/29/P2023112900269.htm (accessed July 16, 2025).
(69) Wang, X.; Chen, L.-W. A.; Ho, K.-F.; Chan, C. S.; Zhang, Z.; Lee, S.-C.; Chow, J. C.; Watson, J. G. Comparison of Vehicle Emissions by EMFAC-HK Model and Tunnel Measurement in Hong Kong. *Atmos. Environ.* **2021**, *256*, 118452.
(70) H.K. OBSERVATORY. The Year's Weather—2023. https://www.hko.gov.hk/en/index.html (accessed June 17, 2025).
(71) Transport Department of Hong Kong. *Monthly Trffic and Transport Digest*; Transport Department, 2023.
(72) WHO Regional Office for Europe. Review of Evidence on Health Aspects of Air Pollution, 2013. https://www.ncbi.nlm.nih.gov/books/NBK361805/(accessed Oct 11, 2025).
(73) Richmond-Bryant, J.; Owen, R. C.; Graham, S.; Snyder, M.; McDow, S.; Oakes, M.; Kimbrough, S. Estimation of On-Road NO2 Concentrations, NO2/NOX Ratios, and Related Roadway Gradients from near-Road Monitoring Data. *Air Qual., Atmos. Health* **2017**, *10* (5), 611−625.
(74) Wu, Y.; Song, G. The Impact of Activity-Based Mobility Pattern on Assessing Fine-Grained Traffic-Induced Air Pollution Exposure. *Int. J. Environ. Res. Public Health* **2019**, *16* (18), 3291.
(75) Navarro-Martínez, A.; Hajji, M.; Armengol, J. M.; Soret, A.; Ponce-de-León, M.; Valencia, A. The Effect of Recurrent Mobility on Air Pollution Exposure and Mortality Burden in Catalonia. *Int. J. Health Geogr.* **2025**, *24* (1), 19.
(76) Welch, B. L. The Generalization of Student's Problem When Several Different Population Variances Are Involved. *Biometrika* **1947**, *34* (1/2), 28.
(77) Mann, H. B.; Whitney, D. R. On a Test of Whether One of Two Random Variables Is Stochastically Larger than the Other. *Ann. Math. Stat.* **1947**, *18* (1), 50−60.
(78) Greer, F.; Thaneya, A. B.; Horvath, A. Environmental Justice and Systems Analysis for Air Quality Planning in the Port of Oakland in California. *Environ. Sci. Technol.* **2024**, *58* (19), 8135−8148.
(79) U.S. Census. New York—Census Bureau Profile, 2023. https://data.census.gov/profile/New_York?g=040XX00US36 (accessed July 18, 2025).
(80) Population Education. Densest Neighborhoods In The World. https://populationeducation.org/densest-neighborhoods-in-the-world/(accessed July 21, 2025).
(81) Transport and Housing Bureau of Hong Kong. Public Transport Strategy Study, 2017. https://www.td.gov.hk/filemanager/en/publication/ptss_final_report_eng.pdf (accessed Jan 06, 2026).
(82) Yang, W.; Zacharias, J. *Choosing Between Tram and Metro in Hong Kong − Utility*; Affect and Demographics, 2017; pp 131−141.
(83) H.K. Environment and Ecology Bureau. Green Transformation Roadmap of Public Buses and Taxis, 2024. https://www.eeb.gov.hk/sites/default/files/pdf/Bus_Taxi_Roadmap_leaflet.pdf (accessed July 24, 2025).
(84) Biswal, A.; Singh, V.; Malik, L.; Tiwari, G.; Ravindra, K.; Mor, S. Spatially Resolved Hourly Traffic Emission over Megacity Delhi Using Advanced Traffic Flow Data. *Earth Syst. Sci. Data* **2023**, *15* (2), 661−680.
(85) Li, Y.; Zheng, J.; Dong, S.; Wen, X.; Jin, X.; Zhang, L.; Peng, X. Temporal Variations of Local Traffic CO2 Emissions and Its Relationship with CO2 Flux in Beijing, China. *Transp. Res., Part D Transp. Environ.* **2019**, *67*, 1−15.
(86) Griswold, J. B.; Sztainer, T.; Lee, J.; Madanat, S.; Horvath, A. Optimizing Urban Bus Transit Network Design Can Lead to Greenhouse Gas Emissions Reduction. *Front. Built Environ.* **2017**, *3*, 5.
(87) Boriboonsomsin, K.; Tanvir, S.; Barth, M. Modeling the Impacts of Low Emission Zone on Route Diversion and Emissions of Heavy-Duty Trucks: A Southern California Case Study. *J. Transport. Res. Board* **2024**, *2678* (1), 794−805.
(88) Dennis-Bauer, S.; Pahwa, A.; Jaller, M. Explicit Consideration of Human Exposure to Minimize Freight Routing Impacts. *Transp. Res., Part D Transp. Environ.* **2026**, *151*, 105133.
(89) Chow, W. S.; Liao, K.; Huang, X. H. H.; Leung, K. F.; Lau, A. K. H.; Yu, J. Z. Measurement Report: The 10-Year Trend of PM 2.5 Major Components and Source Tracers from 2008 to 2017 in an

https://doi.org/10.1021/acs.est.5c14619
Environ. Sci. Technol. XXXX, XXX, XXX−XXX

Urban Site of Hong Kong, China. *Atmos. Chem. Phys.* **2022**, *22* (17), 11557−11577.
(90) Louie, P.; Watson, J.; Chow, J.; Chen, A.; Sin, D.; Lau, A. Seasonal Characteristics and Regional Transport of PM in Hong Kong. *Atmos. Environ.* **2005**, *39*, 1695.
(91) Ryu, B. Y.; Jung, H. J.; Bae, S. H. Development of a Corrected Average Speed Model for Calculating Carbon Dioxide Emissions per Link Unit on Urban Roads. *Transp. Res., Part D Transp. Environ.* **2015**, *34*, 245−254.
(92) Abou-Senna, H.; Radwan, E.; Westerlund, K.; Cooper, C. D. Using a Traffic Simulation Model (VISSIM) with an Emissions Model (MOVES) to Predict Emissions from Vehicles on a Limited-Access Highway. *J. Air Waste Manage. Assoc.* **2013**, *63* (7), 819−831.

https://doi.org/10.1021/acs.est.5c14619
Environ. Sci. Technol. XXXX, XXX, XXX−XXX